Ore Geology Reviews 72 (2016) 963–988

Contents lists available at ScienceDirect

Ore Geology Reviews

journal homepage: www.elsevier.com/locate/oregeorev

# The Archean BIF-hosted Lamego gold deposit, Rio das Velhas greenstone belt, Quadrilátero Ferrífero: Evidence for Cambrian structural modification of an Archean orogenic gold deposit

Breno de Souza Martins [a,*], Lydia Maria Lobato [a], Carlos Alberto Rosière [a], Steffen G. Hagemann [b], João Orestes Schneider Santos [b], Fernando Lucas dos Santos Peixoto Villanova [c], Rosaline Cristina Figueiredo e Silva [a], Lucas Henrique de Ávila Lemos [c]

[a] Universidade Federal de Minas Gerais, Avenida Antônio Carlos, n.° 6627, Bairro Pampulha, Belo Horizonte, Minas Gerais, CEP 31270-901, Brazil
[b] School of Earth and Environment, The University of Western Australia, 35, Stirling Highway, Crawley, WA 6009, Australia
[c] AngloGold Ashanti Córrego do Sítio Mineração S/A, Mina do Lamego, Sabará, Minas Gerais, Brazil

ARTICLE INFO

*Article history:*
Received 5 May 2015
Received in revised form 21 August 2015
Accepted 26 August 2015
Available online 25 September 2015

*Keywords:*
Lamego deposit
Lamego BIF
Rio das Velhas greenstone belt
Quadrilátero Ferrífero
Orogenic gold deposit

ABSTRACT

The Lamego orogenic gold deposit (1.3 Mt measured resources at 7.26 g/t Au) is located at the south-western end of the 5 km-long Cuiabá–Lamego trend, Quadrilátero Ferrífero region, Brazil. Both Archean orogenic gold deposits are situated in the Rio das Velhas greenstone belt with the lithological succession at Lamego consisting of metamorphosed (greenschist facies) mafic volcanic rock, chert and banded iron formation (BIF), and carbonaceous and micaceous pelites. The Lamego fold, which controls the Lamego deposit, is the most visible structure related to the $D_1$–$D_2$ event, with a perimeter of about 4.8 km and a maximum width of 450 m. The fold is defined by the layering of the mafic unit with minor BIF and large exposures of carbonaceous and micaceous pelites. It is a rootless, reclined, isoclinal, cylindrical fold with an axial trace striking northwest–southeast dipping 20° to 30°. The hinge zone is thickened and the limbs are thinned, with the limbs dipping 20° to 30° to the SE. Orebodies consist of the Lamego BIF, where gold-mineralized zones are related to iron-rich bands, and associated silicification zones. Replacement-style mineralization is associated with sulfide bands; mainly pyrite, As-rich pyrite, and arsenopyrite. Two structural generations, $G_1$ and $G_2$, are recognized and encompass a set of structural elements. The $G_1$ structural generation developed in a progressive deformation event and resulted in structures oriented from NE to SW and dipping to the SE. Structures pertaining to the $G_2$ structural generation are oriented N–S dipping to the W. The four major high-grade gold orebodies are Carruagem, Queimada, Arco da Velha, and Cabeça de Pedra. Their gold grade shows a spheroidal pattern and a distribution that varies along the $S_{1-2}$ foliation. These lenses represent the hinge zone of $F_2$ reclined folds with the plunge of the orebodies controlled by the $F_2$ fold axes. The lower-grade gold lenses are controlled by pinch and swell, and locally expressed quartz boudins developed during $D_1$–$D_2$. They have two orthogonal directions, one to the NW–SE and the other to the NE–SW, thereby defining chocolate-tablet style boudinage. Hydrothermal monazite grains in a mineralized mafic volcanic rock indicate that mineralization formed at 2730 ± 42 Ma (U–Pb SHRIMP). Younger monazite dated at 2387 ± 46 Ma, and xenotime dated at 518.5 ± 9 Ma suggest Siderian and Cambrian imprint in the Lamego deposit area. The Cambrian age reflects the late stages of the Brasiliano orogenic cycle, which is expressed in the Lamego deposit by the $S_3$ crenulation cleavage (trend NS and dip steeply to the E). Importantly, the Cambrian structural modification is responsible for the present geometry of the Lamego orebodies, but is not associated with hydrothermal alteration; it has not introduced any new gold and also has not caused remobilization of the orebodies or ore minerals.


## 1. Introduction

Orogenic gold deposits are structurally controlled. In most Archean cases the orebody shape is controlled by the structures formed late in the tectonic evolution of the terrain in which the deposit is emplaced (Bierlein et al., 2006; Goldfarb et al., 2005; Groves et al., 1998; Hagemann and Cassidy, 2000; Kerrich et al., 2000, 2005). These authors further emphasize that orebodies and ore textures are largely undeformed, and thus interpreted as being related to the last structural–hydrothermal event that caused the precipitation of gold and associated hydrothermal alteration minerals. For this reason, individual orebodies display the original geometry at the time of formation and, therefore, lack any post ore deformation or remobilization. On the other hand,

* Corresponding author.
*E-mail address:* brenosouzamartins@yahoo.com.br (B. de Souza Martins).

http://dx.doi.org/10.1016/j.oregeorev.2015.08.025
0169-1368/

hypozonal gold deposits in Archean terrains that display structural and hydrothermal alteration similarities to orogenic gold systems provide evidence for major remobilization of sulfides and gold. These include examples such as Hemlo in the Superior province (Tomkins et al., 2004); Challenger in the South Australian craton (Tomkins and Mavrogenes, 2002), and Griffins Find in the Yilgarn craton (Tomkins and Grundy, 2009; Hagemann and Gill, 2011). In these deposits the timing of gold precipitation is interpreted to be pre-peak (Archean) metamorphism.

Nowadays, Brazil is classified as the 12th largest gold producer with 2600 t in reserves and production, with 56.7 t of gold exploited by gold companies, and 10.1 t of gold mined by artisanal miners (gold diggers) (Thiers et al., 2014). Furthermore, Minas Gerais state is the largest gold producer in Brazil with 52.4% of the production and 28.0% of the reserves (Lima and CAR, 2014).

The Quadrilátero Ferrífero (QF) region is one of Brazil's most important gold provinces with historical production and present gold reserves exceeding 1000 t (Vial et al., 2007a). Vial et al. (2007a) reported that during the 18th and 19th centuries, the QF was the largest gold producer in the world, including the world-class Morro Velho and Cuiabá deposits (Fig. 1), presently owned by AngloGold Ashanti Córrego do Sítio S/A (AGA). The Morro Velho gold mine started production in 1834, and has a cumulative production of about 470 t (15 Moz) of gold (Vial et al., 2007b). The Cuiabá gold mine contains 150 t, 5 Moz produced until 2015 and more than 7 Moz in mineral resources (AGA, personal communication).

The Cuiabá–Lamego gold trend is significantly endowed in gold (11 Moz produced) and shares most of the structural complexities that generally characterize orogenic gold style mineralization in the QF, where Archean ore systems underwent Proterozoic structural modifications (e.g., Baltazar and Zucchetti, 2007).The QF structural evolution is defined by three main periods with a complex structural arrangement. The first between 2.8 and 2.67 Ga verging to NNE, the second between 2.1 and 1.9 with fold and thrust belts verging to the NW, and the third from 650 to 500 Ma verging to the W.

The present investigation on the orogenic Lamego deposit, which is part of the Cuiabá–Lamego gold trend within the Rio das Velhas greenstone belt, in the QF of Brazil (Fig. 1), provides a detailed documentation of an Archean orogenic gold system that was affected by the Transamazonian orogenic event (Brito Neves, 2011; "Minas accretionary orogeny" most recently proposed by Teixeira et al., 2015), and the 630–480 Ma Brasiliano orogenic events (Alkmim and Marshak, 1998; Baltazar and Zucchetti, 2007; Lobato et al., 2007; Pedrosa-Soares et al., 2011). Significantly, the gold orebodies hosted along the Lamego fold (Fig. 3a, b, c) lack characteristics of remobilization textures, but the Archean orebody geometry was significantly modified by Cambrian age folds and thrusts.

The aims of this paper are to: (1) characterize the geological setting of the Lamego deposit including the lithostratigraphy and mineralization styles; (2) provide a detailed structural documentation of the four separate Lamego gold orebodies via detailed underground mapping of several levels; (3) constrain the chronology of structural events and orebody geometries based on the careful documentation of structures in 3-D and cross-cutting relationships; (4) provide geochronological evidence for Archean and Proterozoic timing of mineralization and structures, respectively; (5) introduce a descriptive geological model that is compatible with all the documented geological and geochronological observations; and (6) compare and contrast the structural setting and control of the Lamego gold orebodies with classic orogenic gold deposits in Brazil and worldwide.

## 2. Regional geological setting

The QF is located in the southern portion of the São Francisco Craton (Almeida, 1977) and the stratigraphic subdivision was established by Dorr (1957, 1969) who subdivided the region into: (i) Archean granite–gneissic complexes, older than 2.9 Ga (Machado and Carneiro, 1992; Machado et al., 1989); (ii) Rio das Velhas Supergroup (Figs. 1 and 2), an Archean greenstone belt sequence dated between 3.0–2.7 Ga, (Machado and Carneiro, 1992; Machado et al., 1989); and (iii) Proterozoic Minas Supergroup, Itacolomi Group and Espinhaço Supergroup (Dorr 1957, 1969).

The granite–gneiss terrain is composed of tonalite–trondjhemite–granodiorite (TTG). These consist of 3.2 Ga dome-like granite–gneiss domains associated with intercalations of amphibolites and metasedimentary rocks (Ladeira, 1980a; Lana et al., 2013; Schorscher, 1988), which are intruded by metatonalites, metandesites, metagranites, pegmatites and Proterozoic mafic dikes (Carneiro et al., 1994; Noce, 1995; Noce et al., 2005). Noce et al. (2007) suggest that these TTG derive from igneous protoliths older than 2.9 Ga.

The Archean Rio das Velhas greenstone belt (Fig. 2) covers approximately 4000 km$^2$ in the QF, and is divided into the basal Nova Lima and top Maquiné Groups (Dorr 1957, 1969; Oliveira, 1984). The Nova Lima comprises ultramafic rocks, basic lavas, graywackes and sandstones, with intercalations of BIF, quartz–dolomite and quartz–ankerite rocks, conglomerates and carbonaceous pelites (Baltazar and Zucchetti, 2007; Dorr, 1969). The Nova Lima Group hosts a large number of gold deposits (Ladeira, 1980b; Lobato et al., 2001a, 2001b; Lobato and Vieira, 1998a, 1998b), including Lamego (Martins, 2011; Martins et al., 2011). The Maquiné Group is divided into the basal Palmital (O'Rourke, 1957) and top Casa Forte Formations (Gair, 1962), the former with sandstone and quartz pelite, and the latter with sandstone and conglomerate (Dorr, 1969). The greenstone belt sequence was mainly metamorphosed to the greenschist facies. A thorough review of the literature from the last century focused on this greenstone belt is found in Baltazar and Zucchetti (2007).

Baltazar and Pedreira (1998), Baltazar and Silva (1996), Baltazar and Zucchetti (2007), and Pedreira and Silva (1996), subdivide the Rio das Velhas Supergroup from bottom to top into seven lithofacies associations. For the Nova Lima Group these are the: (i) mafic–ultramafic volcanic, (ii) volcanic–chemical, (iii) clastic–chemical, (iv) volcaniclastic, and (v) resedimented associations. For the Maquiné Group, the (vi) coastal, and (vi) non-marine associations are indicated. These are developed into four sedimentary cycles that were formed between 2.8 and 2.6 Ga (Noce et al., 2007). The platformal Minas Supergroup sequence unconformably lies over the Rio das Velhas Supergroup, and is subdivided into the Caraça, Itabira, Piracicaba and Sabará Groups (Dorr, 1969).

The QF region is characterized by a complex structural arrangement, with Archean basement domes surrounded by large synclines where the Minas Supergroup rocks dominate (Dorr, 1969; Alkmim and Marshak, 1998).

Baltazar and Zucchetti (2007) have proposed that the structural evolution of the QF region took place in three main periods, corresponding to the Rio das Velhas Orogeny. The earliest period occurred between 2.8 and 2.67 Ga, corresponding to the evolution of the Rio das Velhas greenstone belt; the second period between 2.1 and 1.9 Ga, related to the Transamazonian event in the Proterozoic; the third period between 650 and 500 Ma, in the Neoproterozoic, related to the Brasiliano orogeny. No consensus exists on how many deformational events the Rio das Velhas Supergroup experienced (see summary in Table 1).

Alkmim and Marshak (1998) proposed three main deformational phases to the Proterozoic tectonic evolution (Minas accretionary orogeny by Teixeira et al., 2015). The first episode generated fold and thrust belts with a NE–SW trend, verging to NW, during the Rhyacian (2.1–2.0 Ga). The second phase is related to the Paleoproterozoic orogenic collapse, caused by a regional extensional tectonic event, resulting in the uplift of the Archean granite–gneiss domes and formation of the regional synclines (the dome-and-keel structure of Marshak and Alkmim, 1989). The third event is related to the Neoproterozoic Brasiliano orogeny (0.7–0.45 Ga), and was responsible for the formation of fold and thrust belts verging to the west (Alkmim and Marshak, 1998).

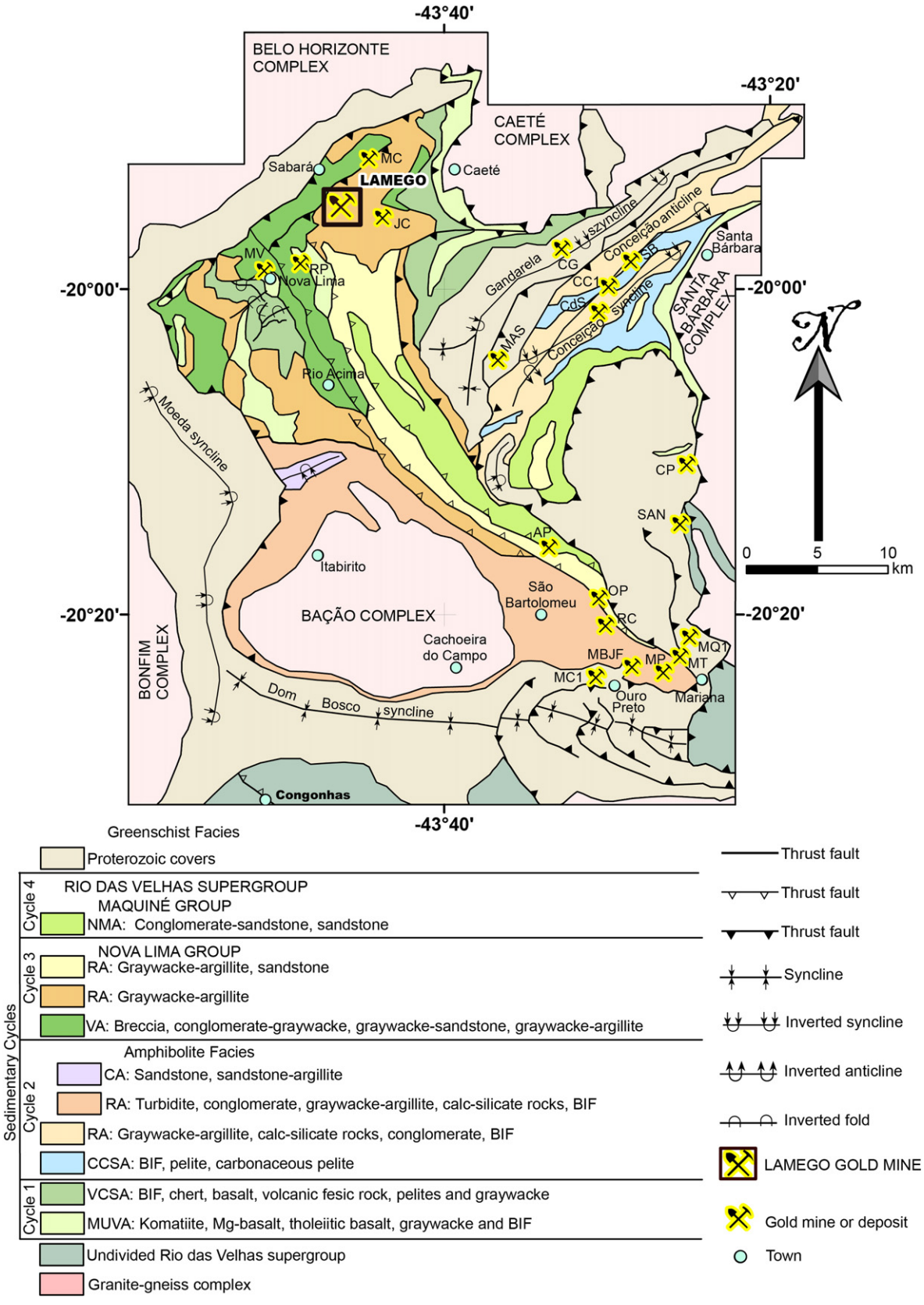


**Fig. 1.** Simplified geological–structural map of the Quadrilátero Ferrífero region showing the location of the Lamego deposit. The Rio das Velhas greenstone belt is separated in lithofacies associations. MUVA —mafic–ultramafic volcanic, VCSA — volcanic–chemical sedimentary, CCSA — clastic–chemical sedimentary, RA — resedimented, CA — coastal, VA — volcaniclastic, NMA — non-marine associations. Other gold deposits associated with the Rio das Velhas greenstone belt and the Minas Supergroup are also shown. The gold deposits hosted by the greenstone belt are: CdS — Mina Córrego do Sítio, MC — Mina Cuiabá, MV — Morro Velho, RP — Raposos, SAN — Santo Antônio, SB — São Bento, JC — Juca Vieira. On the other hand, deposits associated with Minas Supergroup are: AP — Antônio Pereira, CC1 — Conceição, MQ1 — Maquiné, MT — Mata Cavalo, MBJF — Mina Bom Jesus das Flores, MAS — Mina Santo Antônio, AP — Antônio Pereira, OP — Ouro Preto, CP — Cata Preta, MP — Mina da Passagem, RC — Rocinha, and CG — Congo Soco.
Modified after Baltazar and Zucchetti, 2007.

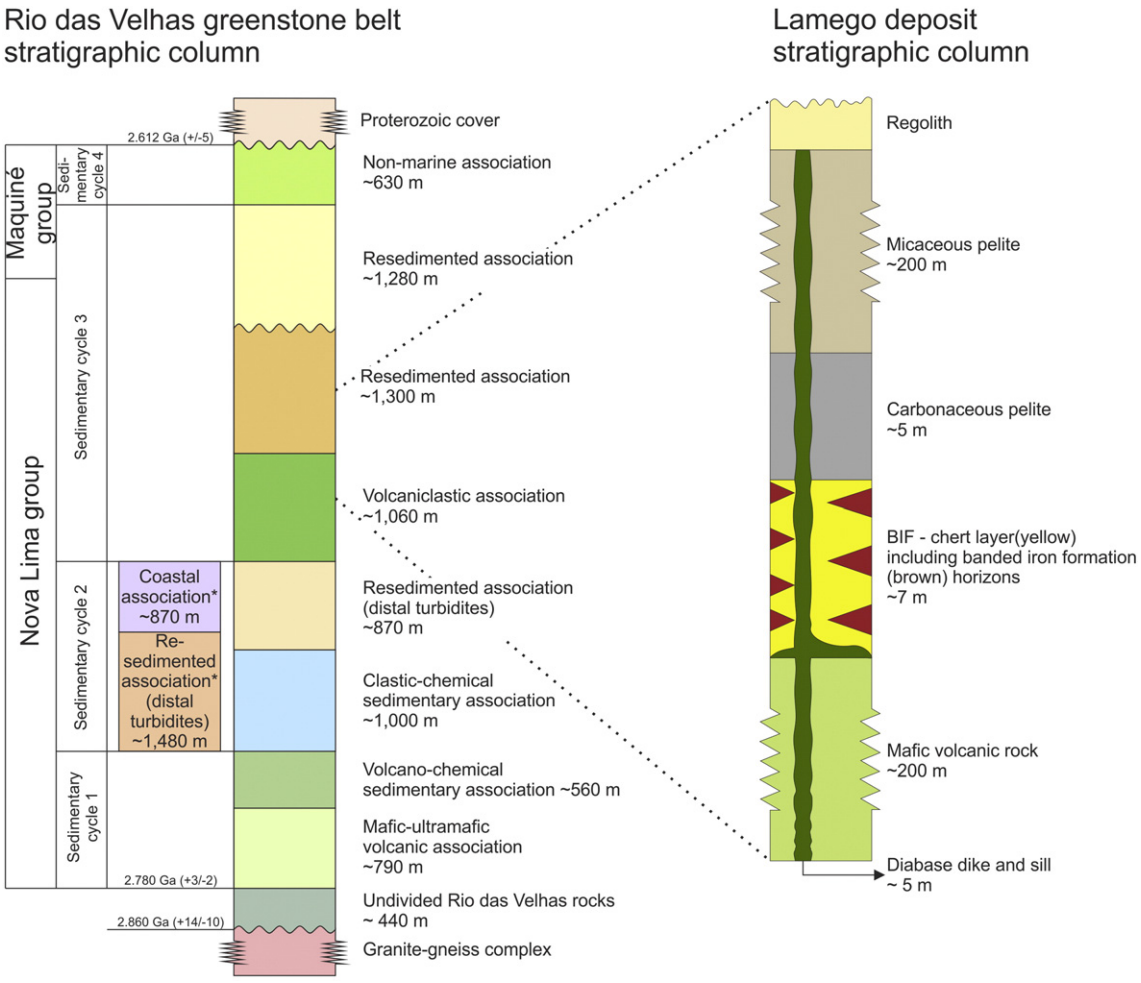


**Fig. 2.** Schematic stratigraphy of the Lamego deposit area based on geological mapping (Fig. 3), combined with the regional stratigraphic column proposed for the Rio das Velhas greenstone belt by Baltazar and Zucchetti (2007). Note that the lithological column at Lamego is related to the resedimented association of the sedimentary cycle 3, and the rock thicknesses do not correspond to those of the regional stratigraphy.

## 3. Lamego deposit: history and production

Exploration at Lamego started between 1985 and 1990, with the identification of several mineralized zones hosted in metachert and BIF. Three promising areas were selected, and named Arco da Velha, Queimada and Cabeça de Pedra orebodies (Fig. 3). In 2001, a new drilling campaign targeted the Carruagem orebody and produced positive results, which supported further exploration efforts. Only in

**Table 1**
Proposal of QF structural evolution by Marshak and Alkmim (1989); Alkmim and Marshak (1998), and Baltazar and Zucchetti (2007).

| Eon (Ga) | Archean | | 2,5 | 2,0 | Proterozoic | 1,5 | 1,0 | 0,5 | Fanerozoic |
|---|---|---|---|---|---|---|---|---|---|
| Orogeny | | Jequié | | Transamazonian | | | | Brasiliano | |
| Alkmim and Marshak (1989, 1998) | Continental crustal fragments older than 3.2 Ga served as basement of Rio das Velhas greenstone belt<br>Formation of Minas basin into a ensialic or passive-margin basin | | | $D_1$ compressional event<br>NW-vergent<br>Thin-skinned tectonics<br>$D_2$ extensional event<br>Oceanic basin<br>Rift-type ensialic basin<br>$D_3$ collapse/ extensional even<br>Dome-and-keel tectonics | | | | $D_4$ compressional event<br>W-vergent<br>Thrust-fold belt | |
| Baltazar and Zucchetti (2007) | $D_{1Reg}$ compressional simple shear event<br>N to S tectonic transport<br>E-striking, S-verging thrust faults<br>S-verging tight to isoclinal folds, with ENE-plunging axes and open, flexural folds<br>Axial–planar $S_1$ foliation, subparallel to folded $S_0$ (355/65)<br>Down-dip stretching and mineral lineation, intersection lineation ($S_0$ and $S_1$) parallel to fold axes<br>$D_{2Reg}$ compressional simple shear event<br>NE to SW tectonic transport<br>NW-striking thrust faults (03–050/40–60)<br>NW trending, SW-verging tight to isoclinal folds<br>Axial–planar $S_2$ foliation (060/35; mylonitic foliation)<br>Stretching lineation, mineral lineation (060–070/20–30) | | | $D_{3Reg}$ extensional event<br>WNW to ESE tectonic transport<br>Nucleation of regional synclines and onset of Minas Supergroup deposition<br>Uplift of granite–gneissic basement as metamorphic core complexes<br>Normal faults around the complexes | | | | $D_{3Reg}$ extensional event<br>WNW to ESE tectonic transport<br>Nucleation of regional synclines and onset of Minas Supergroup deposition<br>Uplift of granit-gneissic basement as metamorphic core complexes<br>Normal faults around the complexes | |

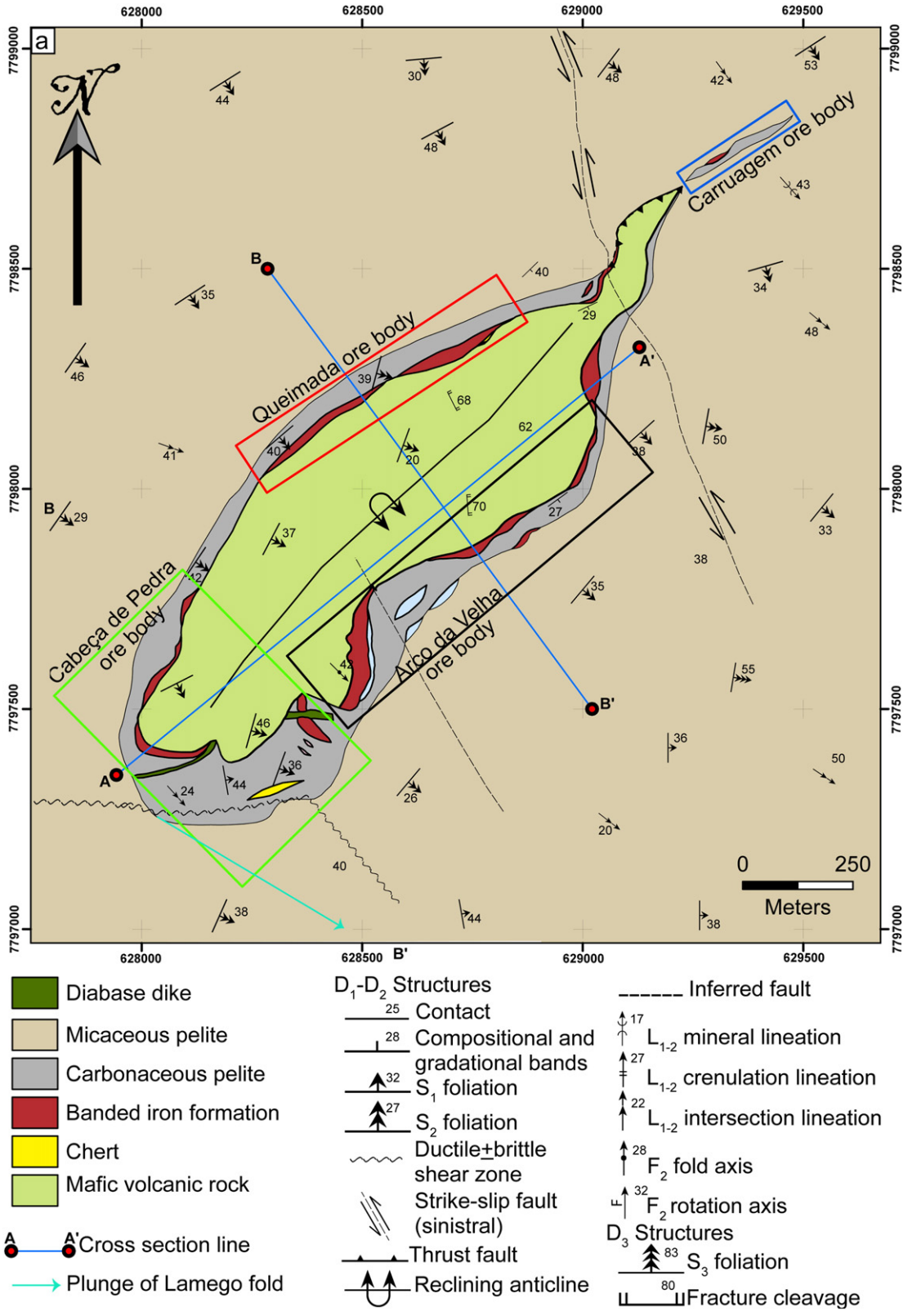


**Fig. 3.** (a) Geological map of the Lamego open pit mine showing the four orebodies, where the macrostructure is represented by a reclined anticline. It has 4.8 km of outcropping perimeter, with NW–SE axis orientation. The overturned limb is the Queimada orebody (red), the normal limb is the Arco da Velha orebody (black), the hinge zone is the Cabeça de Pedra orebody (green), and the limb junction is the Carruagem orebody (blue). (b) NE–SW cross section cutting the Cabeça de Pedra and Arco da Velha orebodies showing the folded Lamego structure. (c) NW–SE cross section cutting the Queimada and Arco da Velha orebodies.
Panel (a) is modified after Villanova (2011).

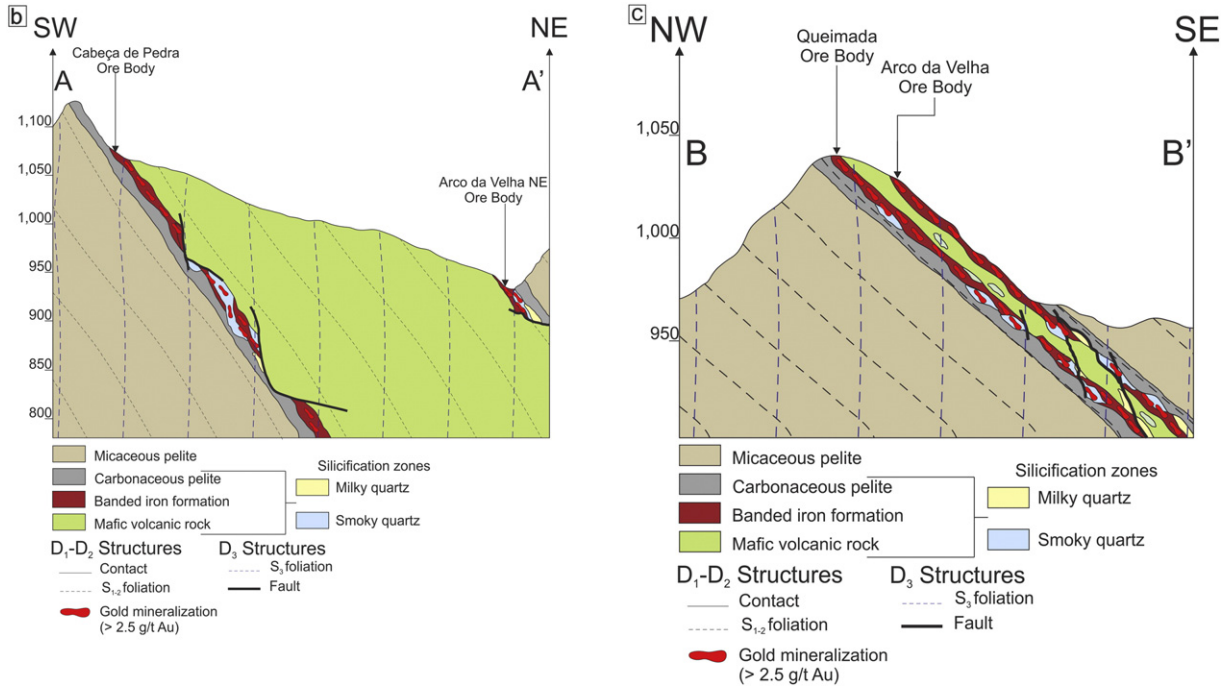


**Fig. 3** (*continued*).

2009 did the Lamego Project result in the establishment of the Lamego mine with the mine life estimated to extend to 2026.

More recently, in October 2014, AGA reported Lamego to have 250,000 t gold measured reserves and 1.3 Mt measured resources, with an average grade of 7.26 g/t Au and a cut-off grade of 2.68 g/t Au (Table 4). The Lamego ore is processed together with the Cuiabá ore, at the gold plant that has a total annual capacity of 1.7 Mt with a 93% recovery (AGA, personal communication).

## 4. Methodology

### *4.1. Underground geological mapping, petrography and structural analyses*

Detailed underground geological mapping at 1:100 scales was undertaken at eight mine levels intersecting the Queimada orebody level 1, the Arco da Velha and Cabeça de Pedra orebodies, both levels 1 and 2, and Carruagem orebody levels 1, 2 and 5.1, although the paper focuses on this latter orebody.

Recorded structural data include compositional banding, lithological contacts, foliations, veins, boudins, lineations, folds and thrust/shear zones. These data were used to build the structural evolution of the Lamego deposit in a regional context. In addition, seventy thin sections were made from seven diamond drill holes in order to establish the relationship between lithology, structure and gold mineralization.

### *4.2. Indirect and implicit 3D model*

To understand the orebody geometry, gold distribution and the relationship between lithology, and structures, a 3D model of the orebodies was built using the Lamego AGA drillhole database. This model was combined with underground geological maps to highlight the structural behavior of the ore zones. Gold was analyzed via fire assay, with each sample weighing 30 g; samples with results of fusion obtained by ICP-AAS greater than 30 g/t Au were redone using gravimetric analysis.

The Collar survey, geology and assay data were imported into the software package Leapfrog Geo® (version 2.1), and indirect and implicit lithological and grade shell models were built. The indirect method was chosen because of the high geological complexity of the host rocks in the ore zone.

It is considered good practice to do isotropic interpolation (= no preferred orientation) and isosurfacing as a first step into an implicit 3D lithological model to keep the modeling result as objective as possible (Hill et al., 2014, 2013; Vollgger et al., 2013). We interpolated the Au assay values assigned to the drill-hole intervals, and used spheroidal interpolation, since the linear interpolation tended to create unrealistically voluminous isosurfaces in areas of sparse data (Hill et al., 2013, 2014; Vollgger et al., 2013). In order to avoid nugget effects, we have rejected the highest 30% of gold values for the Leapfrog model (Hill et al., 2013, 2014; Vollgger et al., 2013).

For the computational construction of the ore grade shells (implicit 3D assay model), approximately 54,000 assay samples were used. For the purpose of the present study, the grade shells values have been separated in the following ppm Au intervals: (i) low grades between 0.2 and 0.5 ppm; (ii) intermediate grades between 0.5 and 1.5 ppm; and (iii) high grades >1.5 ppm. These are not, however, considered economic grades at the Lamego mine. The interpolation parameters are summarized in Table 2. The histogram of ore grade shells from the four orebodies at Lamego reveal a positively skewed distribution (Fig. 4), which is common for gold assay distribution (Hill et al., 2013; Vollgger et al., 2013).

**Table 2**
Summary of the LEAPFROG interpolation parameter used to build the 3D model.

| Parameters | Values |
|---|---|
| Data transform | Log |
| Variogram model | Spheroidal isotropic |
| Sill | 8.41 |
| Range | 50 m |
| Nugget | 3.00 |
| Drift | Constant (ordinary kriging) |
| Isosurface resolution | 1 m |
| Isosurfaces values | <0.5 ppm |
| | 0.5–1.5 ppm |
| | >1.5 ppm |

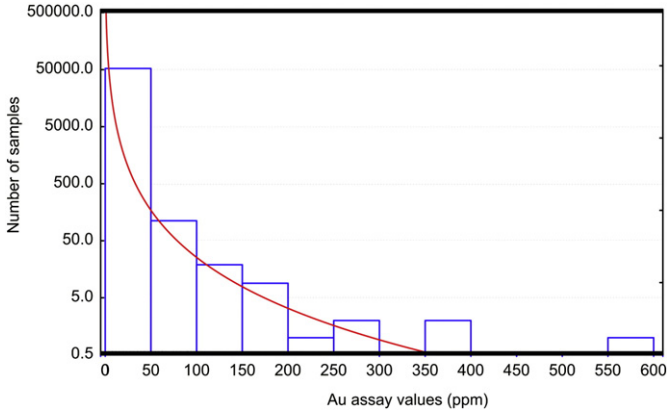


**Fig. 4.** Histogram of gold distribution revealing a positive skewed distribution. Data from AngloGold Ashanti Córrego do Sítio Mineração S/A.

### 4.3. U–Pb SHRIMP analyses

The sample selected (Fig. 5a) for U–Pb SHRIMP analyses represents the sulfide zone of the lower mafic volcanic rock, at level 3 of the Cabeça de Pedra orebody. It was collected to investigate the presence of hydrothermal monazite and xenotime, as both minerals develop along the $S_{1-2}$ foliation.

Eight polished thin sections (Fig. 5b) were initially examined by optical microscope and scanning electron microscope (SEM) located in the Centre for Microscopy, Characterization and Analysis (CMCA), at the University of Western Australia (UWA). The SEM is a TESCAN-VEGA3 equipped with an Oxford Instruments X-Max 50 silicon drift energy dispersive spectrometer (EDS) system with AZtec® and INCA® software. The EDS system was used to identify hydrothermal monazite and xenotime.

The monazite (Fig. 5c) revealed to be much more common than xenotime, but only about 5% of the grains are suitable for U–Pb geochronology, and are thus at least 10 μm in size and lack mineral inclusions. Sections L1, L5, L6, and L7 contain the best grains, which were removed by micro-drilling. This generated 22 plugs of 1 mm and 3 mm in diameter that were organized in two epoxy mounts (N14-06 and N14-07). The U–Th–Pb analyses were carried out at the Sensitive High Resolution Ion MicroProbe — SHRIMP II (B) — at Curtin University of Technology, Western Australia, following the analytical procedures described by Foster et al. (2000). The primary ion current was ~0.4 nA, and each analysis consisted of six scans of the isotopic spectrum formed by 13 masses: $^{202}LaPO_2$, $^{203}CePO_2$, $^{204}Pb$, $^{204}Background$, $^{205.8}NdPO_2$, $^{206}Pb$, $^{207}Pb$, $^{208}Pb$, $^{232}Th$, $^{245}YCeO$, $^{254}UO$, $^{264}ThO_2$, and $^{270}UO_2$. Because the composition and amount of Th and U of monazite was unknown prior to the analyses, three standards were analyzed: French (Paquette et al., 1994), Z2234 (Fletcher et al., 2010; Stern and Sanborn, 1998), and Z2908 (Stern and Sanborn, 1998). During the analytical session, the Z2234 standard (1026 Ma; 200 ppm U; 6000 ppm Th) revealed to be closest to the composition of the Lamego monazite, and was established as the main standard for the Pb/U and Pb/Th calibrations.

Xenotime is present only in section L5 (mount N14-06) as three grains of about 12 μm in diameter (Fig. 5d). Xenotime analyses were performed in another analytical session, where the primary $O_2$-beam was about ≤0.3 nA, using eight scans for each analysis of nine masses: $^{194}Y_2O$, $^{204}Pb$, $^{204}background$, $^{206}Pb$, $^{207}Pb$, $^{208}Pb$, $^{238}U$, $^{248}ThO$, and $^{254}UO$. Xenotime standards MG-1 and Xeno1 were analyzed in another mount (B99), which was gold coated together with mount N14-06. The Pb/U and U content calibration standard was MG1 (490 Ma; U = ±1000 ppm), whereas Xeno1 (997 Ma; Stern and Rainbird, 2001) was used to monitor the $^{207}Pb/^{206}Pb$ ratio. The SHRIMP operating procedures followed those of Fletcher et al. (2004) for xenotime, and Fletcher et al. (2010) for monazite. Data reduction was carried out using Squid 2.5 (Ludwig, 2009) and plots prepared using Isoplot 3 (Ludwig, 2003). Analytical details are given in Table 3.

## 5. Geological setting of the Lamego gold deposit

### 5.1. Lithostratigraphy

The Lamego deposit is hosted by metamorphosed volcanic–sedimentary rocks of the Nova Lima Group, which is represented by a concordant lithostratigraphic package (Fig. 2). The orebodies are disposed along the Lamego fold (Fig. 3a, b, c; Lobato et al., 2013; Martins, 2011; Martins et al., 2011).

From bottom to top the deposit's stratigraphy comprises metabasalt (chlorite–carbonate–sericite–quartz schists), banded chert layers with BIF that are both carbonaceous and/or ferruginous, and carbonaceous and micaceous phyllites, with mineral paragenesis compatible with the greenschist facies mineralogy. The rocks are metamorphosed (Fig. 2); hence, the prefix "meta" applies to rock names but is hereafter omitted for brevity.

#### 5.1.1. Mafic volcanic rock

Green, fine-grained and massive mafic volcanic rock is the oldest unit exposed in the core of the Lamego deposit (Fig. 2). The best exposures are located at level 1 of the Queimada, Arco da Velha and Cabeça de Pedra orebodies. They are up to 200 m thick (Salles, 1998), with a lateral extent of approximately 1.7 km; this rock may exhibit chert layers up to 1 m thick (Fig. 4a).

In foliated portions, the mafic rock is defined by sericite and carbonate schists that encircle sigmoidal aggregates mainly formed by pyrite, where an anastomosed fabric and crenulated trails developed (Fig. 6a).

If present, the pre-hydrothermal paragenesis includes plagioclase, amphibole, epidote, and titanite. Plagioclase is partly replaced by hydrothermal carbonate, quartz, and sericite, whereas the mafic minerals are mainly replaced by chlorite (Fig. 6b).

#### 5.1.2. The Lamego chert and banded iron formation (Lamego BIF)

Chert bands vary from light creamy to dark colored, the latter impregnated by carbonaceous matter, and may contain centimeter-thick carbon films. Ferruginous chert usually contains very fine siderite (rarely magnetite), where this rock may locally grade into true BIF (defined by >15% Fe-content: Brandt and Gross, 1972; James, 1954; Percival, 1954). In this paper, both chert and BIF bands are referred to as the Lamego BIF.

Locally in the BIF bands, a 15- to 20-cm thick, foliated and sulfidized mafic horizon is intersected in the Cabeça de Pedra orebody level 2. The relationship between the amount of chert bands and true BIF varies for each orebody. In the Arco da Velha, Cabeça de Pedra and Carruagem orebodies chert dominates BIF over 50%. For the Queimada orebody the relationship is inverted, with BIF dominating over 50%. The chert beds can be up to 2 m thick, with the best exposure in level 2 of the Arco da Velha orebody, and level 1 of the Cabeça de Pedra orebody.

The Lamego BIF is associated with volcanic rocks and is thus compatible with Algoma-type BIF (Gross, 1980; Gross, 1965). The thickness of the BIF ranges between 1 to 8 m (Salles, 1998), whereas the lateral extent of the BIF horizon is discontinuous and extends up to 500 m in length (Fig. 4a).

The bands of the Lamego-BIF are characterized by alternating, dark carbonate–quartz (±magnetite) and light quartz–carbonate bands (Fig. 6c, d). The BIF is comprised of quartz, carbonate, chlorite, sericite, pyrite, arsenopyrite, pyrrhotite (and minor chalcopyrite, galena and sphalerite), and accessory minerals such as sericite, rutile and carbonaceous matter (Fig. 6e, f).

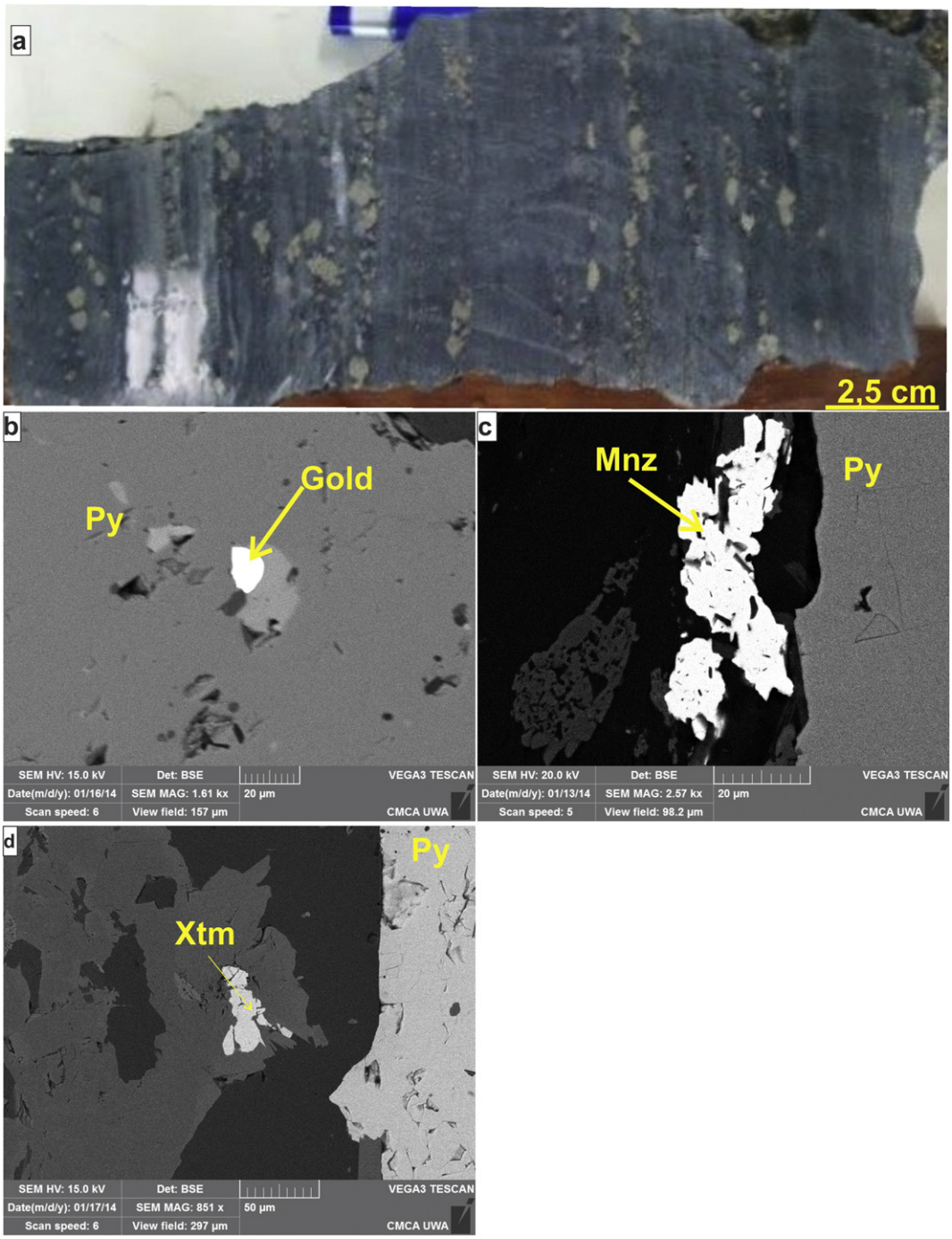


**Fig. 5.** Sample of sulfidized mafic volcanic rock used in the geochronological studies (see text for detailed description). (a) Polished hand sample with representative sulfide veins from the Cabeça de Pedra orebody level 3. Back-scattered EDS images of pyrite (Py) in sulfide veins, exhibiting gold inclusion (b), associated hydrothermal monazite (Mnz) (c) and xenotime(Xtm) (d).

*5.1.3. Pelitic rocks*

Carbonaceous and micaceous pelites (Fig. 6g, h) are at the top of the stratigraphic succession in the Lamego deposit. They envelop the entire Lamego deposit, with the carbonaceous pelite being 1 to 5 m thick, and the micaceous pelites up to 200 m thick (Salles, 1998). Both have a lateral extent of up to 1.7 km (Fig. 4a).

The carbonaceous pelites (Fig. 6g) are dark, finely laminated, thinly bedded, and made up of carbonaceous matter, quartz, chlorite, carbonate and minor sericite. Locally, these rocks form 0.50- to 1-m thick lenses in the mafic rock and BIF.

The greenish to light grayish, micaceous pelites (Figs. 2 and 6h) overlie the carbonaceous pelites; they are laminated and display gradational and compositional stratification. The micaceous pelites contain sericite, muscovite, quartz, carbonate and subordinate amounts of carbonaceous matter.

*5.1.4. Diabase intrusions*

These are exposed mainly in the Carruagem orebody level 1, and in the Cabeça de Pedra open pit (Fig. 3a). They may be parallel to or cross-cut both carbonaceous and micaceous pelites, and BIF. They extend for about 200 m with an average width of up to 5 m. These are fine-grained textured, green rocks, and although foliated near the contacts with wall rocks, they grade to medium grained over short distances towards the core of the intrusion, where the foliation is not prominent. The dikes and sills are composed of green hornblende, actinolite–tremolite, epidote, chlorite, carbonate, plagioclase, sericite

**Table 3**
. U–Pb zircon and xenotime crystals, Lamego gold deposit.

| SPot | U ppm | Th ppm | Th U | $^{206}$Pb ppm | $^{208}$Pb ppm | $4f^{206}$ % | Isotopic ratios | | | | | Ages | | | Disk.% |
|---|---|---|---|---|---|---|---|---|---|---|---|---|---|---|---|
| | | | | | | | $^{207}$Pb/$^{206}$Pb | $^{207}$Pb/$^{235}$U | $^{206}$Pb/$^{238}$U | Error correl. | $^{208}$Pb/$^{232}$Th | $^{208}$Pb/$^{232}$Th | $^{206}$Pb/$^{238}$U | $^{206}$Pb/$^{207}$Pb | |
| *Monazite* | | | | | | | | | | | | | | | |
| a.1-1 | 37 | 21,157 | 587 | 7 | 579 | 8.55 | 0.13138 ± 5.26 | 5.8774 ± 35.3 | 0.2053 ± 9.76 | 0.276 | 0.0305 ± 2.93. | 608 ± 18 | 1204 ± 107 | 2887 ± 551 | 63.6 |
| c.1-1 | 36 | 29,410 | 839 | 3 | 698 | 11.94 | 0.24249 ± 5.95 | 2.0384 ± 26.1 | 0.0864 ± 8.45 | 0.324 | 0.0265 ± 3.28 | 528 ± 17 | 534 ± 43 | 2568 ± 412 | 82.3 |
| d.1-1 | 57 | 13,646 | 246 | 13 | 558 | 17.75 | 0.32699 ± 8.49 | 7.2345 ± 26.9 | 0.2612 ± 8.34 | 0.310 | 0.0461 ± 3.34 | 901 ± 30 | 1496 ± 111 | 2833 ± 417 | 52.7 |
| e.1-1 | 44 | 22,345 | 520 | 11 | 804 | 5.18 | 0.16739 ± 4.81 | 7.7494 ± 19.1 | 0.2755 ± 7.66 | 0.401 | 0.0401 ± 3.56 | 796 ± 28 | 1568 ± 107 | 2859 ± 285 | 50.6 |
| h.1-1 | 63 | 8344 | 136 | 17 | 292 | 5.19 | 0.23060 ± 2.61 | 8.2212 ± 8.48 | 0.3085 ± 4.88 | 0.576 | 0.0393 ± 3.32 | 774 ± 25 | 1733 ± 74 | 2770 ± 114 | 42.5 |
| h.1-2 | 133 | 7450 | 58 | 49 | 450 | 3.03 | 0.20851 ± 1.53 | 10.9391 ± 4.96 | 0.4252 ± 3.77 | 0.760 | 0.0678 ± 4.85 | 1317 ± 62 | 2284 ± 72 | 2712 ± 53 | 18.7 |
| h.1-3 | 77 | 5469 | 73 | 17 | 210 | 6.47 | 0.20954 ± 8.15 | 6.8930 ± 13.3 | 0.2682 ± 8.23 | 0.620 | 0.0434 ± 6.30 | 854 ± 53 | 1532 ± 112 | 2711 ± 172 | 48.7 |
| j.1-1 | 59 | 12,102 | 212 | 17 | 546 | 2.00 | 0.16806 ± 4.60 | 8.6872 ± 11.5 | 0.3389 ± 5.08 | 0.443 | 0.0502 ± 3.14 | 992 ± 30 | 1881 ± 83 | 2706 ± 169 | 35.0 |
| m.1-1 | 67 | 7977 | 123 | 24 | 734 | 0.93 | 0.19680 ± 15.4 | 11.9128 ± 15.7 | 0.4213 ± 4.26 | 0.270 | 0.1026 ± 3.11 | 1975 ± 59 | 2266 ± 81 | 2867 ± 247 | 24.8 |
| m.1-2 | 74 | 7815 | 109 | 24 | 764 | 1.47 | 0.13879 ± 2.37 | 8.0543 ± 6.77 | 0.3848 ± 4.18 | 0.617 | 0.1089 ± 3.05 | 2092 ± 61 | 2099 ± 75 | 2367 ± 91 | 13.3 |
| m.1-3 | 62 | 5486 | 92 | 21 | 497 | 0.57 | 0.15950 ± 2.34 | 8.3306 ± 5.32 | 0.3913 ± 4.21 | 0.792 | 0.1012 ± 3.16 | 1947 ± 59 | 2129 ± 76 | 2395 ± 55 | 13.0 |
| m.1-4 | 34 | 14,168 | 437 | 5 | 526 | 9.36 | 0.27879 ± 4.10 | 4.8590 ± 16.1 | 0.1774 ± 6.54 | 0.406 | 0.0415 ± 7.46 | 821 ± 60 | 1053 ± 64 | 2815 ± 240 | 67.6 |
| *Xenotime* | | | | | | | | | | | | | | | |
| f.1-2 | 500 | 1948 | 4 | 35 | 46 | 0.58 | 0.05924 ± 6.61 | 0.6716 ± 7.36 | 0.0822 ± 3.24 | 0.440 | 0.0265 ± 3.21 | 525 ± 21 | 509 ± 16 | 576 ± 144 | 12 |
| f.1-1 | 801 | 3614 | 5 | 59 | 87 | 2.22 | 0.05734 ± 11.5 | 0.6731 ± 11.9 | 0.0851 ± 3.01 | 0.253 | 0.0278 ± 3.99 | 537 ± 20 | 527 ± 15 | 505 ± 253 | −4.5 |
| f.2-1 | 650 | 2782 | 5 | 47 | 67 | 1.40 | 0.05829 ± 9.06 | 0.6724 ± 9.63 | 0.0837 ± 3.13 | 0.347 | 0.0273 ± 3.60 | 531 ± 20 | 518 ± 16 | 540 ± 199 | 3.7 |

and quartz. The main accessory minerals are titanite and ilmenite (Villanova, 2011).

### 5.2. The Carruagem, Queimada, Arco da Velha and Cabeça de Pedra orebodies at the Lamego deposit

Gold at Lamego is recovered from four orebodies (Fig. 3a, b, c), Carruagem being the most significant, followed by Queimada, Arco da Velha, and Cabeça de Pedra.

The Carruagem orebody (Fig. 7a, b, c) is located in the NE portion of the Lamego fold. It carries the highest gold grades at Lamego, and contains 62% of the reserves. From levels 1 to 5.1, mineralization is predominantly associated with smoky quartz veins. From levels 5.1 to 8, the BIF thickens, and the amount of gold increases proportionately. The underground lithological and structural maps of the Carruagem orebody, at levels 1, 2 and 5.1, show significant geological variations at depth, such as: mafic rocks that dominate in the central portions of the mapped areas; decrease in the volume of BIF; increases in silicification zones from level 1 to 5; and encircling of carbonaceous pelites around silicification zones (see Table 6).

The Queimada orebody is at the overturned limb and is located in the NW of the Lamego fold. It carries the lowest gold grades at Lamego, and is not mined yet. At level 1, mineralization is predominantly associated with BIF.

The Arco da Velha orebody is at the normal limb and located in the SE of the Lamego fold. In level 2, this orebody shows a continuous, mappable chert layer measuring 194.08 $m^2$ and massive sulfide zones associated with a silicification zone totalizing 6.73 $m^2$.

The Cabeça de Pedra orebody is at the hinge zone and is located in the SW of the Lamego fold. This orebody displays the best expression of a continuous mappable chert layer with a thickness ranging between 1 to 2 m, totaling 4976.27 $m^2$, and massive sulfide zones associated with zones of silicification and chert layers, totaling 9.42 $m^2$.

In general, between levels 1 and 2 the silicification zones increase in thickness and volume with depth, while BIF decreases. Faults develop mainly between the mafic volcanic rock and carbonaceous pelites and less with BIF, silicification zones and micaceous pelites. In Table 6, the geological features observed in the geological maps (Fig. 7) are summarized.

### 5.3. Hydrothermal alteration, mineralization styles and location of gold grains

#### 5.3.1. Hydrothermal alteration

Hydrothermal alteration in the BIF-hosted gold deposits of the Nova Lima Group are discussed by Junqueira et al. (2007), Lobato and Vieira (1998a, 1998b), Lobato et al. (2001a), Martins Pereira et al. (2007), Ribeiro-Rodrigues (1998), Ribeiro-Rodrigues et al. (2007),; Vial et al. (2007a, 2007b, 2007c), and Vieira (1991). For the specific case of Lamego, Salles (1998) detailed the hydrothermal alteration of the mafic rock unit. Lobato et al. (2013), Martins (2011), and Martins et al. (2011) described significant silicification in the proximal alteration zones of ore-hosting rocks.

There are three main types of hydrothermal alteration that dominate and affect all rock types. They are represented by quartz, carbonate and sulfide, and developed parallel to the $S_{1-2}$ foliation. These alteration minerals are best exposed in BIF and carbonaceous pelites (Fig. 8a), but less well developed in the mafic volcanic footwall rock and micaceous pelites (Fig. 8b, c).

*Silicification* is the dominant hydrothermal alteration type in the Lamego deposit, containing smoky and milky quartz veins (Fig. 6c, d), and minor carbonates, sericite, pyrite and carbonaceous matter. These zones are characterized by high-modal percentage quartz (>85%). They locally form hydraulic breccias that may or may not be boudinaged. The width ranges between 1 to 35 m, where quartz grains can be >0.5-cm long (Fig. 8a, b, c, d).

**Table 4**
. Total resource of the Lamego deposit, as of October 2013, COG > 2.68 g/t Au.
Source: AngloGold Ashanti Córrego do Sítio Mineração S/A.

| Orebodies | Total resource of LAMEGO deposit — Oct. 2014 (with 2014 depletion) COG > 2.15 g/t | | | | | | | | | | | |
|---|---|---|---|---|---|---|---|---|---|---|---|---|
| | Measured | | | Indicated | | | Inferred | | | Total | | |
| | Tons | Au g/t | Au (Oz) | Tons | Au g/t | Au (Oz) | Tons | Au g/t | Au (Oz) | Tons | Au g/t | Au (Oz) |
| Carruagem | 2,010,374 | 5.96 | 384,913 | 631,907 | 6.63 | 134,603 | 1,038,950 | 5.36 | 178,915 | 3,681,231 | 5.90 | 698,431 |
| Cabeça de Pedra | 299,702 | 4.23 | 40,718 | 1,121,749 | 3.56 | 128,455 | 615,823 | 4.56 | 90,251 | 2,037,274 | 3.96 | 259,424 |
| Arco da Velha | 88,309 | 5.03 | 14,287 | 282,276 | 4.24 | 38,506 | 376,741 | 3.34 | 40,404 | 747,326 | 3.88 | 93,197 |
| Queimada | 4201 | 6.10 | 824 | 496,072 | 5.53 | 88,275 | 558,959 | 5.39 | 96,943 | 1,059,232 | 5.46 | 186,041 |
| Arco NE | 0,00 | 0,00 | 0,00 | 631,907 | 6.63 | 134,603 | 737,392 | 3.26 | 77,244 | 737,392 | 3.26 | 77,244 |
| Total | 2,402,586 | 5.71 | 440,742 | 2,532,004 | 4.79 | 389,839 | 3,327,865 | 4.52 | 483,756 | 8,262,455 | 4.95 | 1,314,338 |

Three quartz generations are present (Fig. 8e): (i) deformed, coarse- to medium-grained smoky quartz as irregular masses, both concordant and discordant, within the mineralized zones; (ii) fine-grained, granoblastic, white and milky quartz, which formed from the recrystallization of smoky quartz, and (iii) milky quartz, particularly in fault zones cutting across generations (i) and (ii).

*Sulfidation* is defined by sulfide veins (5 mm to 7 cm wide; Fig. 8f). They locally replace entire Fe-carbonate-rich bands in the BIF (Figs. 6d and 8g). The sulfides are mostly represented by pyrite, As-rich pyrite, arsenopyrite, less chalcopyrite and sphalerite, and also minor pyrrhotite and galena (Fig. 9a, b, c, d). This alteration zone also contains small amounts of sulfosalt minerals as tennantite–tetrahedrite and nickeline, as well as the phosphate monazite.

*Carbonatization* is defined mainly by ankerite, and is best developed as coarse-grained crystals (up to 2 cm) in BIF (Figs. 6e, f and 8g).

### 5.3.2. Mineralization styles

At least three main gold mineralization styles are identified in the Lamego deposit. In the mineralized BIF, $V_2$ veins dominate (Fig. 6c, d) in association with sulfide replacement of the Fe–carbonate and rare magnetite (Fig. 6d). In the mafic rock and carbonaceous pelites the disseminated style dominates (Fig. 8a).

The *vein style* includes quartz–carbonate ± sulfides veins and quartz boudins, which range in thickness from 2 mm to 5 cm (Figs. 6d and 8a, b, c). These veins crosscut all lithologies, but are best developed in BIF that locally shows stockwork texture. The irregular smoky/milky quartz zones can reach widths of >35 m (Fig. 8d, f, g). Gold grades from ore shells in both veins and quartz zones range from 1.6 to 15.8 ppm, locally attaining 300 ppm.

**Table 5**
Structural elements and evolution of the Lamego gold deposit.

| Chronological Deformational Events | Structures | Geometry |
|---|---|---|
| $G_1$ Structures | Lamego fold | Isoclinal recumbent anticline<br>NW-SE axial trace<br>Dipping 20° to 30° to the SE |
| | $S_0$ gradational and compositional bands | Plunges 29°-41° towards 108°-148° |
| | $S_{1-2}$ foliation | Plunges 28°-42° towards 124°-134° |
| | $L_{1-2}$ Lineations | Plunges 28°-40° towards 128°-155° |
| | $V_1$ veins | Plunges 20°-60° towards 20°-80° |
| | $V_2$ veins | Plunges 20-60 towards 98-160 |
| | $F_2$ | Recumbent folds |
| | $F_2$ fold axes | Plunge 10°-28° towards 90°-160° |
| | Shear zone | Plunge 22°-70° towards 102°-168° |
| $G_2$ Structures | $S_3$ crenulation cleavage | Plunge 80°-90° toward N-S |
| | $L_3$ crenulation lineation | Plunge 30° toward 180° |
| | $F_3$ | Open folds |
| | $F_3$ fold axes | Plunge 15-30 towards 180°-200° |
| | Conjugate pair faults | 15°-75° towards 20-80<br>20°-90° towards 185-240 |

The *replacement style* is typical of BIF, and characterized by the confinement of sulfides to this lithology, where favorable Fe-rich carbonate bands (Fig. 6d, e, f) are replaced by sulfides (Fig. 9a, b, c, d). Gold grades vary from 0.03 to 6.63 ppm, with values as high as 89.0 ppm.

The *disseminated style* is characteristic of the mafic rock unit and carbonaceous pelites (Fig. 8c), with the best exposures located at the Cabeça de Pedra orebody. Disseminated sulfides commonly develop in 5–10-cm-wide shear zones parallel to the $S_{1-2}$ foliation (Fig. 8c). The gold grade ranges from 0.03 to 3.8 ppm.

### 5.3.3. Location of gold grains

Gold grains in sulfide-rich BIF vary from 0.04 to 0.05 mm, and are hosted in pyrite and As-rich pyrite, filling As-rich pyrite and porous pyrite (Fig. 9a, b), along the contacts between carbonate, smoky quartz and arsenopyrite (Fig. 9c, d). In silicification zones gold may be "free", included in pyrite, arsenopyrite, and sphalerite (Fig. 9d), along arsenopyrite edges, and as trails in pyrite.

## 6. Chronology of deformational events at the Lamego deposit

Lobato et al. (2013), Martins (2011),; Martins et al. (2011), and Salles (1998) describe the deformational history at the Lamego deposit. It includes two structural generations, referred to herein as $G_1$ and $G_2$, each one encompassing a set of structural elements.

The $G_1$ structural generation developed in a progressive deformation event and resulted in structures oriented from NE–SW and dipping to the SE. Structures pertaining to the $G_2$ structural generation are oriented N–S dipping to the W.

### 6.1. $G_1$ — first structural generation

The $G_1$ structures include sheared, relict gradational and compositional bands ($S_0$); a penetrative axial–planar foliation ($S_{1-2}$); a lineation ($L_{1-2}$) (mineral, stretching and fold axis); veins ($V_1$ and $V_2$); boudins; pinch-and-swell structures; folds ($F_2$); and shear zones (Table 5).

The Lamego fold is the most visible structure related to the $G_1$ structures, with a perimeter of about 4.8 km and a maximum width of 450 m (Fig. 3a). The fold is defined by the layering of the mafic unit with minor BIF and large exposures of carbonaceous and micaceous pelites. It is a rootless, reclined, isoclinal, cylindrical fold with an axial trace striking northwest–southeast dipping 20° to 30°. The hinge zone is thickened (Fig. 3b) and the limbs are thinned (Fig. 3c), with the limbs dipping 20° to 30° to the SE.

The oldest planar structures at Lamego are the gradational and compositional bands ($S_0$) (Fig. 10a) that represent the sedimentary layering, and the deformation associated with $G_1$ tends to partly or entirely transpose $S_0$. Even with consecutive and intense $G_1$ and $G_2$ deformational events, there are portions of the bands that preserve the primary structures. The lithological contacts between the rocks are normal, folded and sheared, but maintain the normal lithostratigrapy. The pole figures of the compositional bands show that $S_0$ is concentrated in the SE, and dip 29°–41° towards 108°–148° (Fig. 10b).

**Table 6**
Summary of the orebodies characteristics resulted by underground geological mapping.

| Orebody | Structural position in Lamego fold | Levels | Mafic rock | Lamego BIF | Carbonaceous pelite | Micaceous pelite | Silicification zones |
|---|---|---|---|---|---|---|---|
| Carruagem | Limb junction (in NE) | 1 | Center of map | NW portion | Dominates and thickens in NE<br>Thinning out in SW | SW portion | NE portion |
| | | 2 | SW and SE portions | Center of map and less in NE portion | Thick in center and SW of map | Local, in center of map | NE portion |
| | | 5.1 | SW portion and center of map | SE and SW portions | NE and NW portions | – | NE portion and between BIF and carbonaceous pelites |
| Queimada | Overturned limb (in NW) | 1 | Center of map | Dominates the entire map<br>Thick in SE and SW portions<br>Thin in NE and SW portions | Encloses all other lithologies | Local, in NW portion | Only small areas between BIF and carbonaceous pelites |
| Arco da Velha | Normal limb (in SE) | 1 | In footwall of orebody | Dominates the entire map | On top of BIF<br>Also as lenses in BIF | On top of carbonaceous pelites | Restricted to BIF |
| | | 2 | In footwall of orebody | SW portion | Thick in SW and NE | Local in NE portion | Predominance in the NE and center parts of the map<br>Thinning out in SW |
| Cabeça de Pedra | Hinge zone (in SW) | 1 | Center of map | NE, NW and center of map | Thickens from SE to SW | – | SE and SW portions |
| | | 2 | Center of map | SE to SW | Thickens from SE to SW | – | SE to SW portions<br>Local in the NE portion |

The $S_{1-2}$ foliation is the most conspicuous planar structure of the Lamego deposit (Fig. 10c). It is defined by the arrangement of chlorite, sericite, quartz and carbonates. It is best developed in the carbonaceous and micaceous pelites, and in the hydrothermally altered mafic volcanic unit. The $S_{1-2}$ foliation is parallel to sub-parallel in the $S_0$, and dips 28°–42° towards 124°–134° (Fig. 10d).

The $L_{1-2}$ stretching mineral lineation (Fig. 10c) is defined by elongated quartz, carbonate, sericite and sulfides; it is best developed in the mafic unit and in the carbonaceous and micaceous pelites. The $L_{1-2}$ lineation is oriented to E–SE, and plunges 28°–40° towards 128°–155° (Fig. 10d).

The vein system consists mostly of quartz–carbonate–sulfide veins, namely $V_1$ and $V_2$. The $V_1$ veins follow the trend of the spaced cleavage and crosscut all structures (Fig. 10e), whereas $V_2$ veins are folded, and may display pinch-and-swell structures and boudinage (Fig. 10f). Where $V_1$ veins crosscut BIF along hinge zones, the associated minerals migrate along the lateral bands forming the $V_2$ veins and imposing a pseudo-stratification (Fig. 10f). In stereographic projection, $V_1$ veins are oriented in the NE quadrant, and dip 20°–60° towards 20°–80° (Fig. 11a). The $V_2$ veins are oriented in the SE quadrant, and dip 20–60 towards 98–160 (Fig. 11b).

The $F_2$ reclined folds only have a local exposure (Fig. 11c), and have a close to open geometry. In stereographic projection, $F_2$ fold axes plunge 10°–28° towards 90°–160° (Fig. 11d), and are parallel to sub-parallel to mineral lineation $L_{1-2}$. However, the best expression of the $F_2$ fold is displayed in BIF at the Carruagem orebody level 5.1, where folds are also reclined with a close to open geometry, but their axes plunge 5°–20° towards 90°–118°.

A northeast-trending, 1–2-m thick shear zone is oriented parallel to the axial plane of the $F_2$ folds and preferentially developed in all schistose layers with the best exposure in the Carruagem orebody (Fig. 11e; left upper corner of photo). Shear zones are perpendicular to the $F_2$ fold axes, and dip 22°–70° towards 102°–168° (Fig. 11f).

### *6.2. $G_2$ — second structural generation*

The $G_2$ structural generation (Table 5) is composed of the crenulation cleavage ($S_3$), the crenulation lineation ($L_3$), the open fold ($F_3$) and faults.

The $S_3$ crenulation cleavage is defined by sericite, and its expression depends on rock types. The $S_3$ crenulation cleavage is well developed in the micaceous and carbonaceous pelites (Figs. 10a and 12a), and the hydrothermally altered mafic unit. It is poorly developed in BIF, where it appears as $S_3$ spaced cleavage (Fig. 11c). These foliations are oriented N–S/80°–90° (sub-vertical), but can dip less than 60° (Fig. 12b).

The $L_3$ crenulation lineation is defined by the intersection between $S_{1-2}$ foliation and $S_3$ crenulation cleavage (Fig. 12a). In stereographic projection the $L_3$ crenulation lineations appear on a N–S great circle with an average plunge of 30° towards 180° (Fig. 12b).

The $F_3$ open folds (Fig. 12c) are developed in micaceous and carbonaceous pelites showing low amplitudes, with a width of up to 3 m. The $F_3$ fold axes plunge with angles of less than 30°, oriented to S with the azimuth between 180 and 200° (Fig. 12d).

A significant conjugate pair of faults is observed at the Lamego deposit (Fig. 12e). They have northwest–southeast and northeast–southwest orientation, and developed as normal and reverse faults cutting all rocks; locally the faults in the carbonaceous pelite vary their dip angles from 30° to 90°. In stereographic projections (Fig. 12f), these faults show two distinct populations: (i) concentrated to the NE dipping 15°–75° towards 20–80; and (ii) concentrated to the SW, dipping 20°–90° towards 185–240.

## 7. Structural control of orebody geometry

Gold resources for the Lamego deposit are calculated based on the geological characteristics of the orebodies. The general gold grade distribution for the Lamego deposit, including the Carruagem orebody levels 1 and 2, are described below.

The resulting indirect and implicit lithological model reveals an outline marked by the footwall mafic and pelitic rocks that has a general NE direction dipping to the SE; the continuity of these rock types is confirmed to depths below level 5.1. In areas where drill-hole data are lacking, the lithological model is uneven as observed in Fig. 13a.

The trends of the Lamego orebodies vary from NE to SW, and dip to the SE. Their plunge ranges from 22° towards 95° in the Carruagem orebody to 25° towards 120° in the Cabeça de Pedra orebody; the Queimada orebody plunges 29° towards 102°, and the Arco da Velha 25° towards 102° (Fig. 13b).

For the Carruagem orebody level 1, gold grades between 0.2 and 0.5 ppm are measured in all rock types. Intermediate gold grades of 0.5 ppm are restricted mainly to BIF, silicification zones, and less to carbonaceous pelites. These grades in the NE portion are related to fault zones. On the other hand, grades >1.5 ppm are associated with BIF, silicification zones, and also contact zones between carbonaceous pelites with BIF. Areas of equal gold grades (isosurfaces) are interrupted by three NW–SE faults that crosscut these surfaces, resulting in gold grades distributed in two main directions: NE–SW and to N–S both dipping to the SE (Fig. 13c).

As for the Carruagem orebody level 2, gold grades between 0.2 and 0.5 ppm are measured in all rock types. Intermediate gold grades

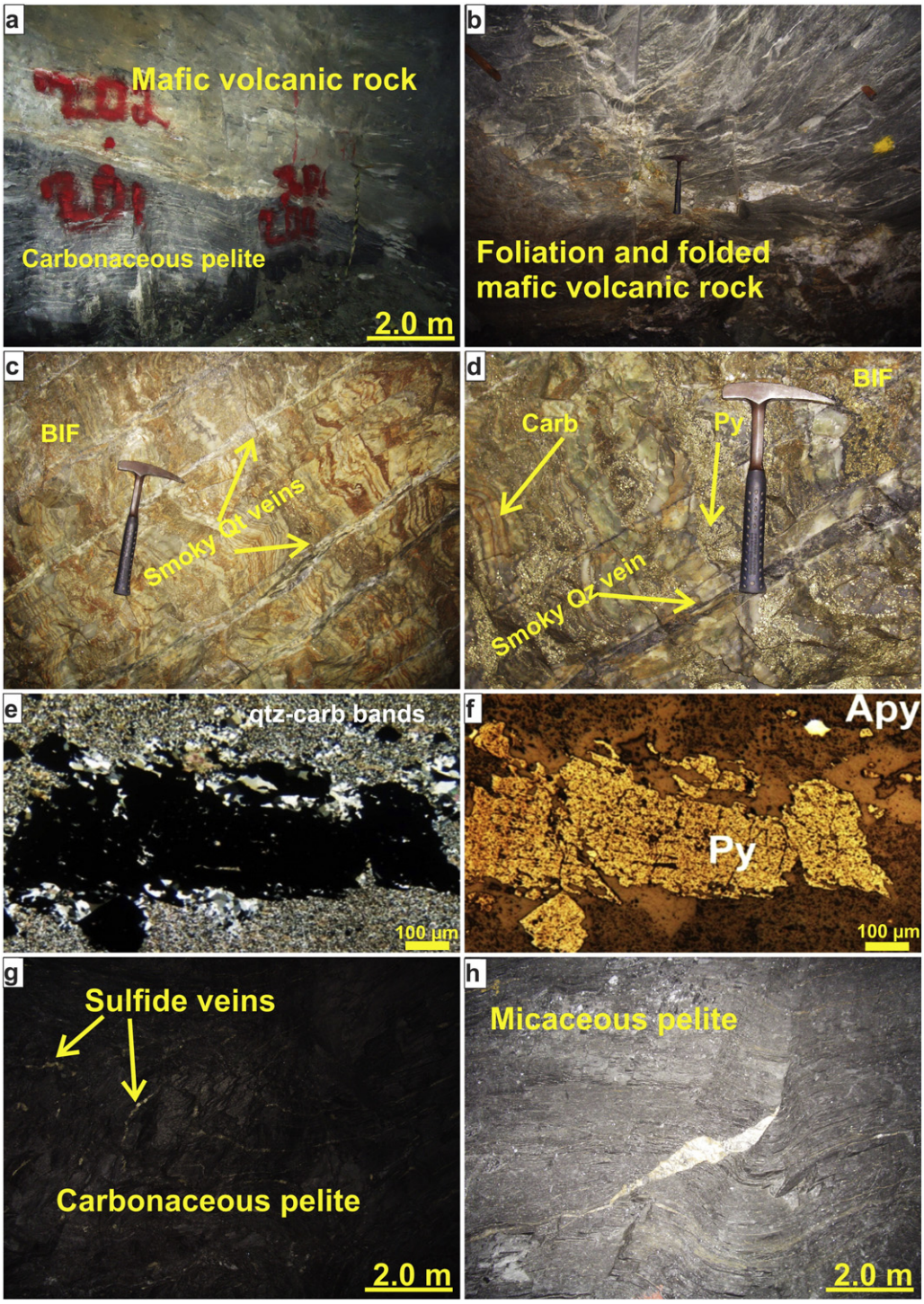


**Fig. 6.** Mafic volcanic rock in a (a) foliated portion in contact with the carbonaceous pelite; Carruagem orebody, level 5.1, Az. 30°, and (b) in a massive and folded portion; Carruagem orebody, level 1, Az. 25°. (c) BIF showing smoky quartz (Qz) veins cutting the bands, systematically characterizing a spaced cleavage. (d) BIF showing smoky quartz (Qz) veins and associated bands with carbonate (Carb) and sulfides, mainly pyrite (Py) (both c and d: Cabeça de Pedra orebody, level 2, respectively Az. 90° and 270°). (e) Photomicrograph of pyrite (Py) and arsenopyrite (Apy) as the main sulfides of BIF; uncrossed nicols, reflected light (200×); (f) Photomicrograph of carbonate (Carb) and smoky quartz (Qz) of BIF; crossed nicols, transmitted light, (200×). (g) Outcrop of carbonaceous pelite, composed mainly by carbonaceous matter, with sulfide veins; Cabeça de Pedra orebody, level 2, Az. 180°. (h) Outcrop of greenish to light grayish, foliated micaceous pelite, with milky quartz sigmoids; Carruagem orebody, level 2, Az. 300°.

of 0.5 ppm are restricted mainly to BIF, silicification zones, and less to carbonaceous pelites. Gold grades >1.5 ppm are associated mainly with fold hinge zones of BIF, coeval to the development of the Lamego fold. However, in the NE portion the silicification zones are dominated by breccia and fault zones with gold grades >1.5 ppm (Fig. 13d).

A section through the Carruagem orebody (Fig. 14a) shows that mineralization is concentrated in several parallel to sub-parallel, 2–5-m thick, irregular tabular ore zones that crosscut the $S_{1-2}$ foliation, and these plunge generally 25–35° towards E to SE. When viewed in sections cut perpendicular to the $S_{1-2}$ foliation (Fig. 14b), high-grade gold lenses show an ellipsoidal pattern and a distribution that varies

along the $S_{1-2}$ foliation plane. On the other hand, when observed in sections cut parallel to the $L_{1-2}$ mineral lineation (Fig. 14c), high-grade gold lenses show a discontinuous distribution, and display a boudinage and pinch-and-swell geometry forming necks.

## 8. SHRIMP U–Pb geochronology

Sample LM-CP is a mineralized sericite–quartz–carbonate ± chlorite ± pyrite schist, and represents the sulfide zone of the lower mafic volcanic rock, level 3 of the Cabeça de Pedra orebody (Fig. 5a). It is intercalated with albite-bearing, sub-parallel, $V_2$ quartz veins. Pyrite with multiple inclusions replaces carbonates, and is mostly associated with quartz veinlets. Gold particles are included in pyrite (Fig. 15a), and the gold grade is close to 0.2 g/t Au.

### 8.1. Monazite

About 30 grains were tested and only 12 analyzed. The majority of the grains are very poor in radiogenic $^{206}Pb$ (3 ppm or less), and also relatively rich in common lead. The analyses of 18 grains were aborted during the first scan. Using a spot size of 10 μm, the resulting 12 analyses were U (average = 62 ppm), and $^{206}Pb$ poor (average = 17 ppm), and also extremely poor in $^{207}Pb$ (average = 3.2 ppm). The small spot size combined with the weak primary beam and the low content of radiogenic $^{206}Pb$ and $^{207}Pb$ produced large uncertainties in the $^{207}Pb/^{206}Pb$ ages (average = 234 Ma).

All data are discordant to highly discordant (discordance from 13% to 82%), where 10 results align in the same regression line intercepting the concordia curve at 2730 ± 42 Ma (2 sigma; MSWD = 0.51) (Fig. 15b).

Two of the monazite grain crystals are younger and align in another regression line, intercepting the concordia curve at 2387 ± 46 Ma. The Lamego monazite grains have much more Th (average = 1.3%) than U, and consequently their main radiogenic lead is $^{208}Pb$ (average = 555 ppm). The Th/Pb ages (uncertainties average = 42 Ma) are more precise than the $^{207}Pb/^{206}Pb$ ages (uncertainties average = 234 Ma), and could provide a better age establishment for the monazite population. However, there was a $^{208}Pb$ loss even stronger than the $^{206}Pb$ and $^{207}Pb$ losses; the twelve $^{208}Pb/^{232}Th$ ages are all scattered between 528 and 2092 Ma. These ages are considered meaningless.

### 8.2. Xenotime

Only three analyses were performed and the results show reasonable U (average = 650 ppm) and high Th contents (Th/U ratios from 4.03 to 4.66). The Pb/U and U calibration used the MG-1 standard (490 Ma; 1000 ppm U). Xeno1 was used to monitor the $^{207}Pb/^{206}Pb$ ratio, but normalization of this ratio was not required because the obtained $^{207}Pb/^{206}Pb$ age (997 Ma) coincides with the age of the standard. The average $^{206}Pb$ is 47 ppm, whereas the average of $^{207}Pb$ is only 2.7 ppm. The low amount of $^{207}Pb$ reflects large uncertainties for the $^{207}Pb/^{206}Pb$ ages (from 144 to 253 Ma), when compared to the uncertainties of the $^{206}Pb/^{238}U$ ages (15 to 16 Ma). The data are concordant and the inverse concordia age is 518.5 ± 9 Ma (MSWD = 0.41; 2 sigma) (Fig. 15c).

## 9. Geological evolution of the Lamego deposit in the QF regional context

The geological evolution of the Lamego deposit is considered in the context of the tectonic framework of the QF, mainly in view of the

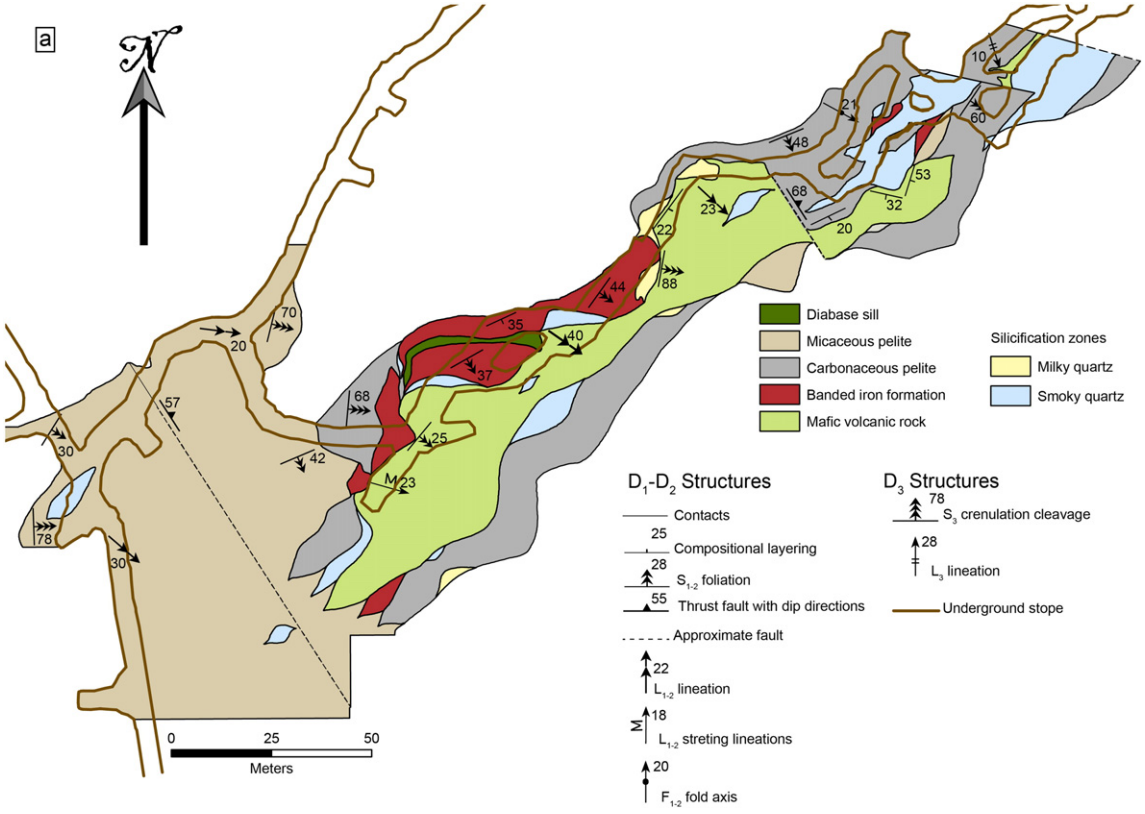


**Fig. 7.** Geological maps of the Lamego underground mine showing 3 levels of the Carruagem orebody. (a) Level 1 elevation 800 m, where BIF dominates the SW and smoky quartz the SE portions of the map, respectively. (b) Level 2 elevation 750 m, where BIF dominates the central portion, while smoky quartz dominates both the SE and SW portions. (c) Level 5.1 elevation 650 m, which corresponds to the SE portion of levels 1 and 2, in this case with an increase in BIF volume and smoky quartz.

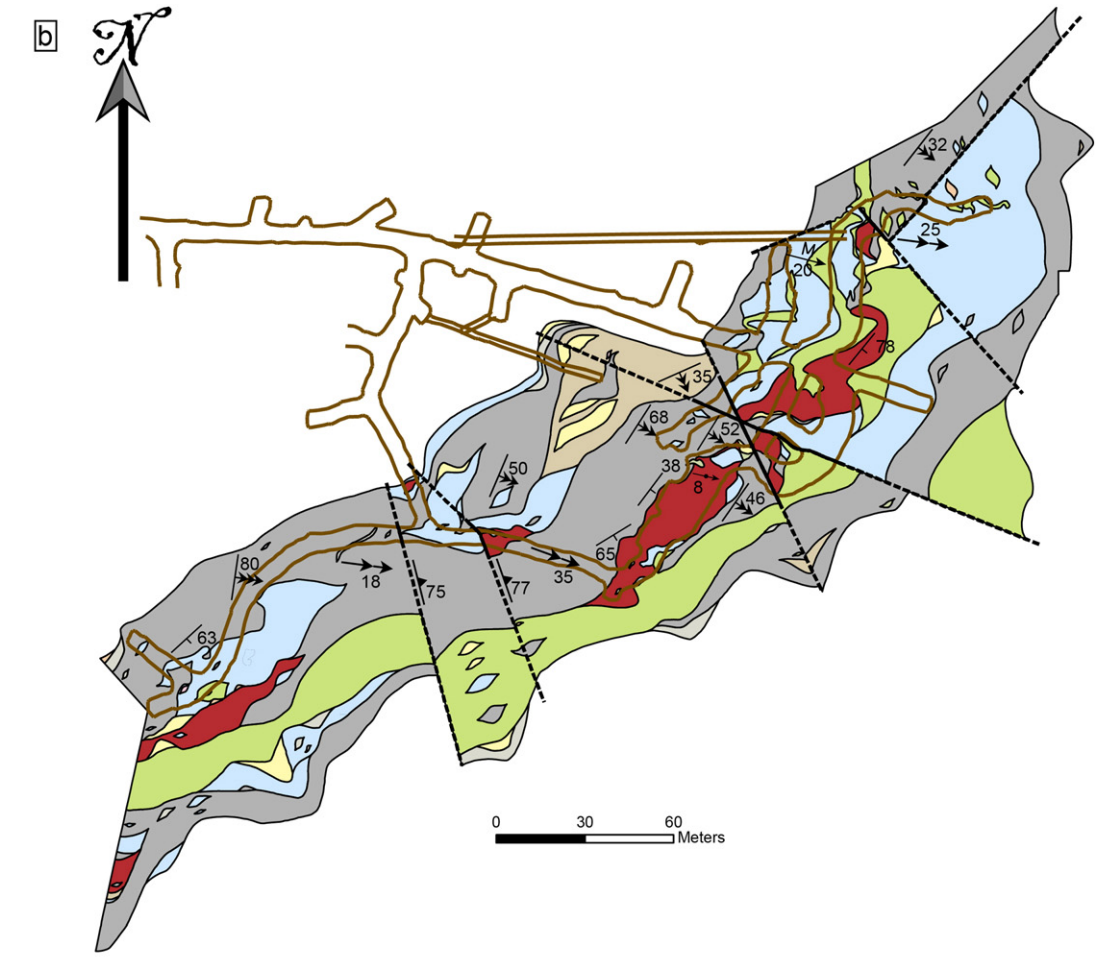



**Fig. 7** (*continued*).

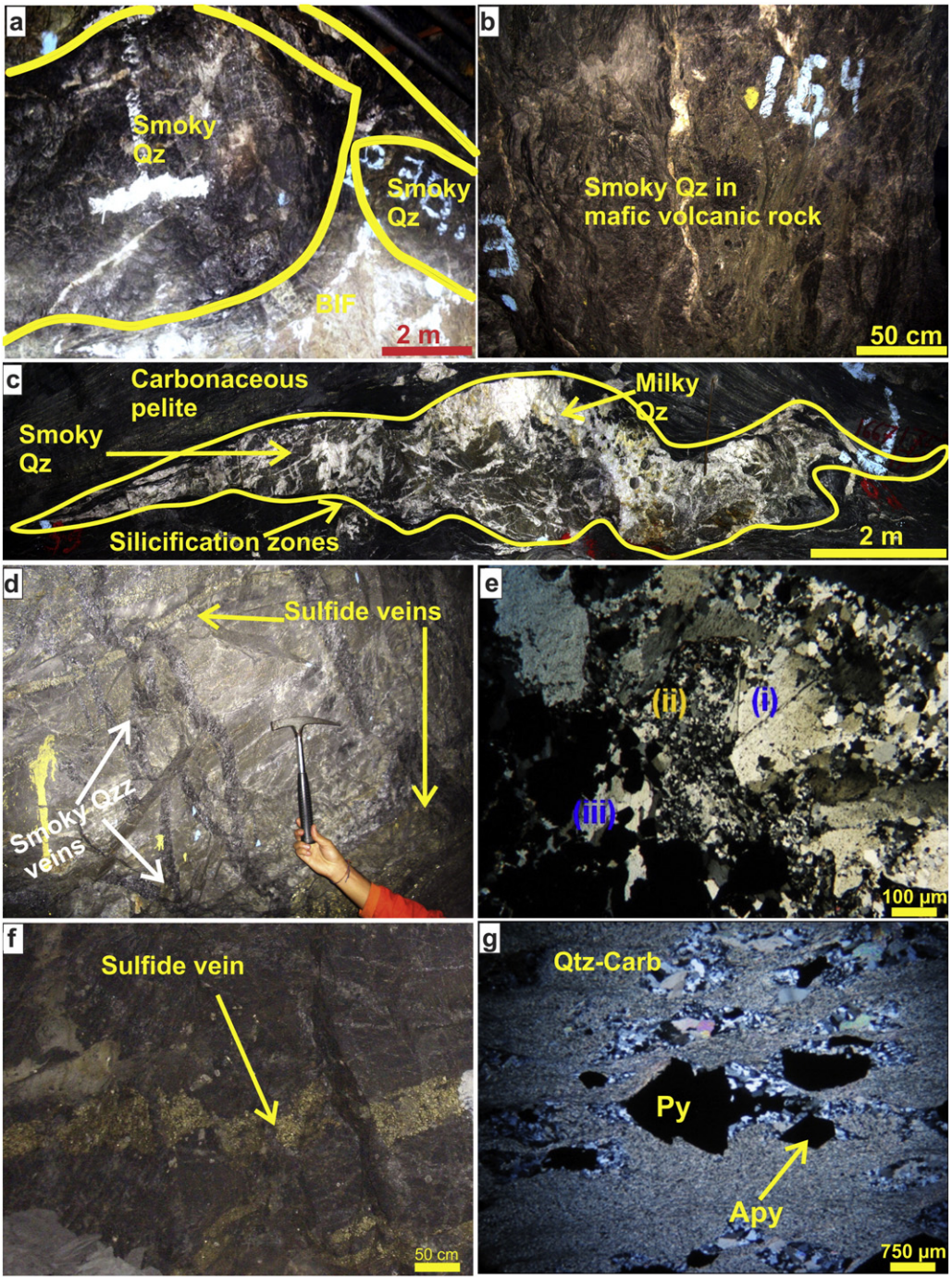


**Fig. 8.** (a) Boudinaged, smoky quartz (Qz) restrained to a fragment of BIF; Carruagem orebody, level 1, Az. 200°. (b) Smoky quartz (Qz) in mafic volcanic rock; Carruagem orebody, level 2, Az. 290°. (c) Sigmoidal, smoky quartz (Qz) in carbonaceous pelite that is structurally controlled by the $S_{1-2}$ foliation; note that the smoky quartz (Qz) turns into milky quartz along the edges; Carruagem orebody, level 1, Az. 190°. (d) Pyrite-dominated silicification zone formed where chert/BIF previously dominated. In detail coarse-grained, smoky quartz (Qz) forms veins that cut the silicification zone and are associated with pyrite (Py); Arco da Velha orebody, level 1, Az. 320°. (e) Photomicrograph of a silicification zone showing three types of quartz: (i) anhedral to locally subhedral, irregular, fractured, medium- to coarse-grained smoky quartz, (ii) fine-grained, polygonal granoblastic quartz, white and milky quartz, developed from the recrystallization of smoky quartz, and (iii) milky quartz, polygonal and subhedral, coarser than (ii); crossed nicols, transmitted light (250×); (f) Pyrite-dominated sulfide veins, in BIF fragment; Arco da Velha orebody, level 1, Az. 350°. (g) Photomicrograph of carbonate (Carb) alteration zone with siderite and associated sulfides, mainly pyrite (Py) and arsenopyrite (Apy); crossed nicols, transmitted light (250×).

new geochronological data presented in this contribution. In particular, we must take into account the 2749–2670 Ma Archean, the Paleoproterozoic (2.22–2.05 Ga; Brito Neves, 2011), and the 630–480 Ma Brasiliano orogenic events (Alkmim and Marshak, 1998; Baltazar and Zucchetti, 2007; Lobato et al., 2007; Pedrosa-Soares et al., 2011).

### *9.1. Archean progressive deformation event and the first structural generation — $G_1$*

At a regional scale, Baltazar and Zucchetti (2007) described a progressive $D_1$–$D_2$ event that is characterized by a NNE to SSW tectonic transport, with folds and faults verging to NNE. The $D_1$ event took place

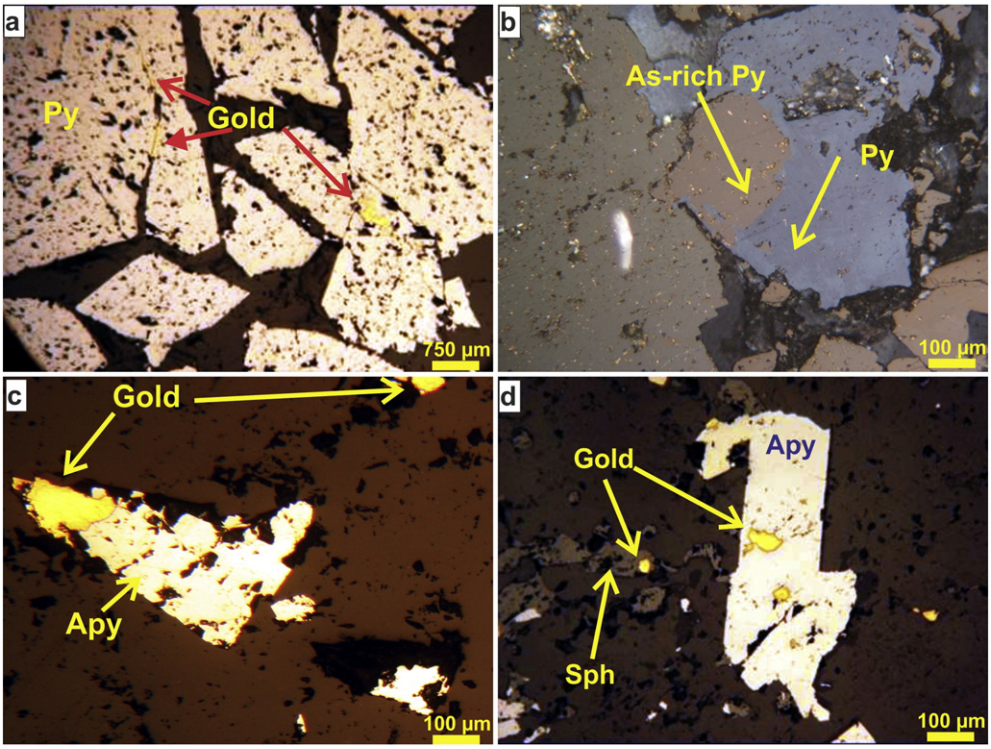


**Fig. 9.** (a) Gold strips associated with porous pyrite (Py), filling fractures and pores; crossed nicols, reflected light (100×). (b) As-rich pyrite and pyrite (Py) in contact; uncrossed nicols, reflected light (200×). (c) Gold associated with arsenopyrite (Apy); crossed nicols, reflected light (200×). (d) Gold particles included in arsenopyrite (Apy), sphalerite (Sph) and smoky quartz (Qz); reflected light, crossed nicols (200×).

between 2749 and 2670 Ma, whereas the progressive $D_2$ event took place at approximately 2700 Ma (Table 3 of Baltazar and Zucchetti, 2007; Lobato et al., 2001a, 2001b; Table 1).

This regional $D_1$–$D_2$ deformation event was responsible for the first generation structures — $G_1$ at the Lamego deposit (Fig. 16a). It is interpreted to have formed the Lamego fold and associated gold mineralization (Fig. 16a).

The $G_1$ structures are understood as progressive because the folds associated with both the $S_0$ compositional bands and $S_{1-2}$ foliation show parallelism and geometrical similarities; these are reclined folds with the axial folds concentrated and plunging to the SE quadrant (Figs. 10b, d and 11d; Martins, 2011; Martins et al., 2011).

The main $G_1$ structures are the $V_1$ and $V_2$ veins, the $S_{1-2}$ foliation, the $L_{1-2}$ mineral lineation, $F_2$ folds, and shear zones that formed along the axial plane of $F_2$ folds. The Lamego $V_1$ veins appear to be the only structural feature related to the commencement of the regional progressive $D_1$ event (e.g., Baltazar and Zucchetti, 2007; Fig. 16a). The veins strike NNS, dip to the NE, and their geometry coincides with regional faults and shear zones (Table 1). Accepting these relations, we interpret the formation of the $V_1$ veins to have started at 2749 Ma (Table 3 of Baltazar and Zucchetti, 2007). As $V_1$ veins evolved to form the $V_2$ veins, during the $G_1$ folding and shearing event, these latter veins develop the same geometry as the $S_{1-2}$ foliation (Fig. 16b), striking to the NE and dipping to the SE.

The continuous development of the $S_{1-2}$ foliation resulted in the formation of metric- to decametric-scale reclined folds, striking to the NE and dipping to the SE (Fig. 11c, d). These folds formed during the NW–SE regional tectonic transport (Fig. 16b; Martins, 2011; Martins et al., 2011).

While the $S_{1-2}$ foliation plane shows a consistent orientation dipping to the SE (Fig. 11c), the trend of the $L_{1-2}$ mineral lineation and fold axes $L_{b1-2}$ is variable (Fig. 11c), indicating a coeval relation between $F_2$ folds and shearing that caused axis rotation, coaxial refolding and disruption of the limbs.

As folds are subsequently flattened, pinch-and-swell structures and boudins are developed (Fig. 16b, c). The final stage of flattening imposes a prolate deformation model, since two stretching directions are established: (i) the longest deformation axis trends NW–SE, which represents the tectonic transport direction during thrusting, and (ii) the intermediate axis trends NE–SW, which represents the lateral escape direction in a triaxial, non-planar deformation. This resulted in a chocolate-tablet, boudin-type structure with two orthogonal stretching directions (cf. Davis and Reynolds, 1996; Ramsay, 1987), developed during the Lamego mineralization (Fig. 14a, b, c; Martins, 2011; Martins et al., 2011).

The deformation related to the first structural generation $G_1$ also gave place to faults and shear zones, disposed along the $F_2$ fold axial plane oriented in the NE–SW direction and dipping to the SE (Fig. 16b, c). These faults and shear zones, associated with $V_1$ and $V_2$ veins, served as hydrothermal fluid pathways in the Archean (Lobato et al., 2007, 2001a, 2001b). Interaction between hydrothermal fluids and host rocks resulted in the precipitation of hydrothermal minerals such as quartz, pyrite, carbonate, sericite, and gold. The richest orebodies represent the loci where the mineralizing fluids were concentrated during folding, resulting in mineralization hosted preferentially in $F_2$ hinge zones and boudins. The $F_2$ fold axes control the plunge of the orebodies (Fig. 13b and 18b, c).

The original $G_1$ structures, responsible for gold mineralization, probably corresponded to the Archean NW–SE Rio das Velhas trend, demonstrated by the new SHRIMP U–Pb monazite age at 2730 ± 42 Ma (MSWD = 0.51) (Table 3, Fig. 15b).

### *9.2. Paleoproterozoic deformation event and its relationship to the first structural generation — $G_1$*

At a regional scale, and following the $D_1$–$D_2$ regional Archean progressive deformation, two other deformation events affected rocks of the QF, namely $D_3$ and $D_4$ (Baltazar and Zucchetti, 2007).

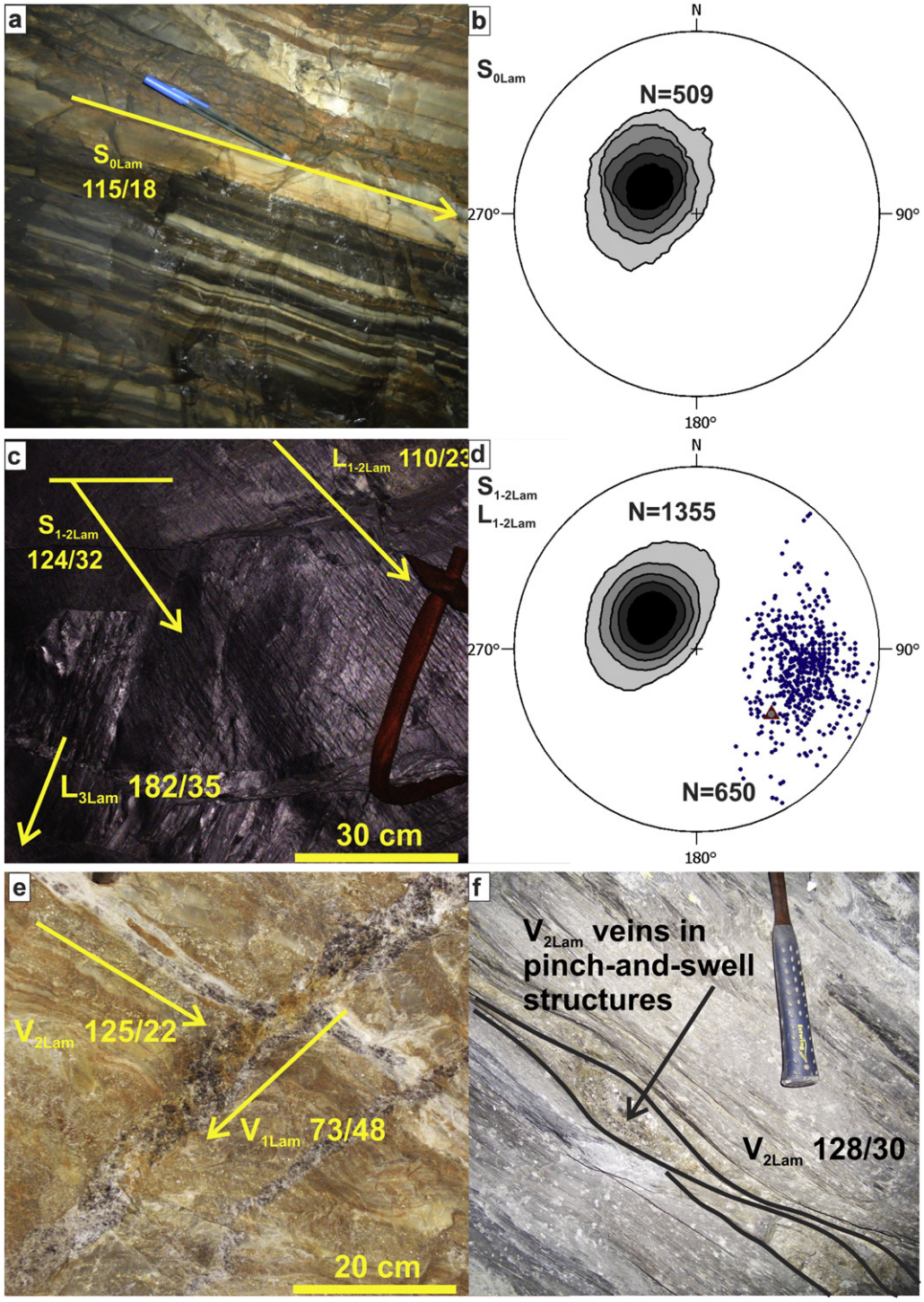


**Fig. 10.** Photo plates showing the relative timing of structural elements and stereographic projection that are displayed by density, equal-angle projection and lower hemisphere. (a) Transposed gradational and compositional $S_0$ bands; Arco da Velha orebody, level 2, Az. 340°. (b) $S_0$ plunge concentrated to the SE. (c) $S_{1-2}$ foliation and $L_{1-2}$ on this plane, with $L_3$ lineation also observed; Arco da Velha orebody, level 1, Az. 15°. (d) $S_{1-2}$ foliation with a geometry similar to the $S_0$ band, and both concentrated in the SE, with the $L_{1-2}$ lineation also plunging to the SE; the brown triangle on the figure represents the foliation intersection. (e) Photo displays a $V_1$ vein following the trend of the spaced-cleavage and crosscutting all structures in BIF; Cabeça de Pedra orebody, level 2, Az. 285°. (f) $V_2$ vein that migrates along the lateral band of a carbonaceous pelite, and imposing a pseudo-stratification; it develops as boudinage that evolves into pinch-and-swell structures; Cabeça de Pedra orebody, level 1, Az. 220°.

The $D_3$ corresponds to the Minas accretionary orogeny (Teixeira et al., 2015), which affected the Minas Supergroup in the Paleoproterozoic (Alkmim and Marshak, 1998; Table 1; Marshak and Alkmim, 1989).

It is noteworthy that Alkmim and Marshak (1998) comment that the Paleoproterozoic NW-verging, thin-skinned thrusting event, compatible with $D_3$ of Baltazar and Zucchetti (2007; Table 1), did not generate a strong regional foliation. The maximum attitude of this foliation has a plunge of 67 towards 111 ($D_1$ of Alkmim and Marshak, 1998; Table 1), with bedding having a maximum plunge of 64 towards 140 (structural data in Alkmim and Marshak, 1998, Fig. 8b), some 5 km NW from Lamego.

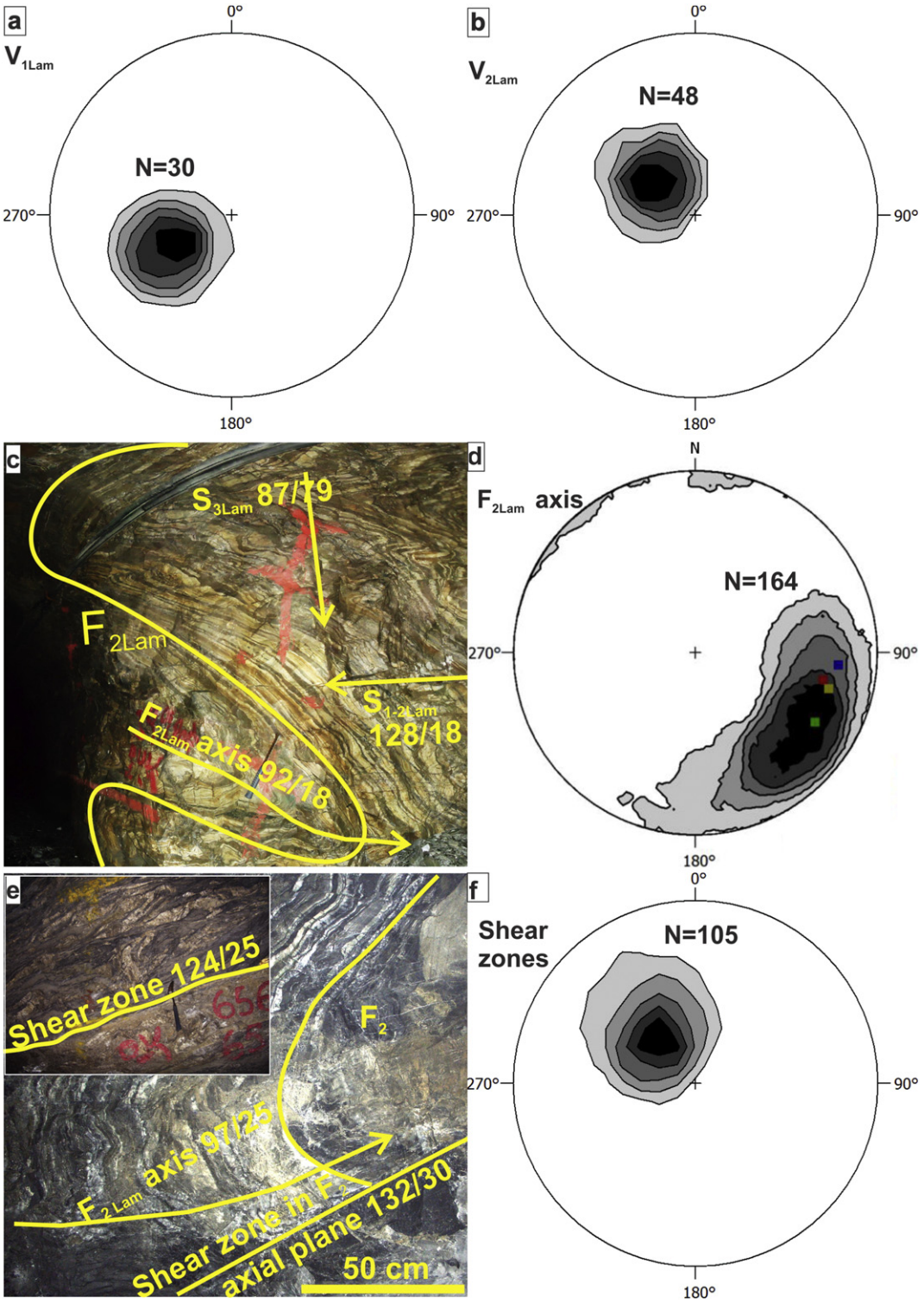


**Fig. 11.** Photo plates showing the relative timing of structural elements and stereographic projection that are displayed by density, equal-angle projection and lower hemisphere. (a) $V_1$ veins oriented in the NE, and (b) $V_2$ veins oriented in the SE. (c) $F_2$ folded BIF with an axis attitude of 92/18. The fold was affected by $S_{1-2}$ foliation in the planar–axial position and by the $S_3$ spaced cleavage; Carruagem orebody, level 5.1, Az. 210°. (d) $F_2$ fold axis concentrated in the SE. The squares indicate the plunge of the orebodies: blue for Carruagem — plunging 22 towards 95; red for Queimada — plunging 29 towards 102; yellow for Arco da Velha — plunging 25 towards 102; and green for Cabeça de Pedra — plunging 25 towards 120. The plunges are concentrated on the main fold axis dispersion. (e) Shear zone oriented parallel to the axial plane of the $F_2$ folds. In detail (left upper corner of photo) note shear zone approximately one-meter thick; Carruagem orebody, level 2, Az. 340°. (f) Shear zones also showing dip to the SE.

These Paleoproterozoic attitudes, both foliation and bedding, are similar for the same structures, $S_{1-2}$ and $S_0$, in our study. They have been ascribed to the first structural generation $G_1$ evolved during the $D_1$–$D_2$ regional deformation events, which are interpreted to be of Archean age. In light of this geometrical similarity, it is likely that the regional $D_3$ foliation is overprinted and parallelized with $S_{1-2}$ foliation ($G_1$ structures) at the Lamego deposit area. Baltazar and Zucchetti (2007) also recognized this regional overprinting in the Cuiabá and Farias gold deposits areas.

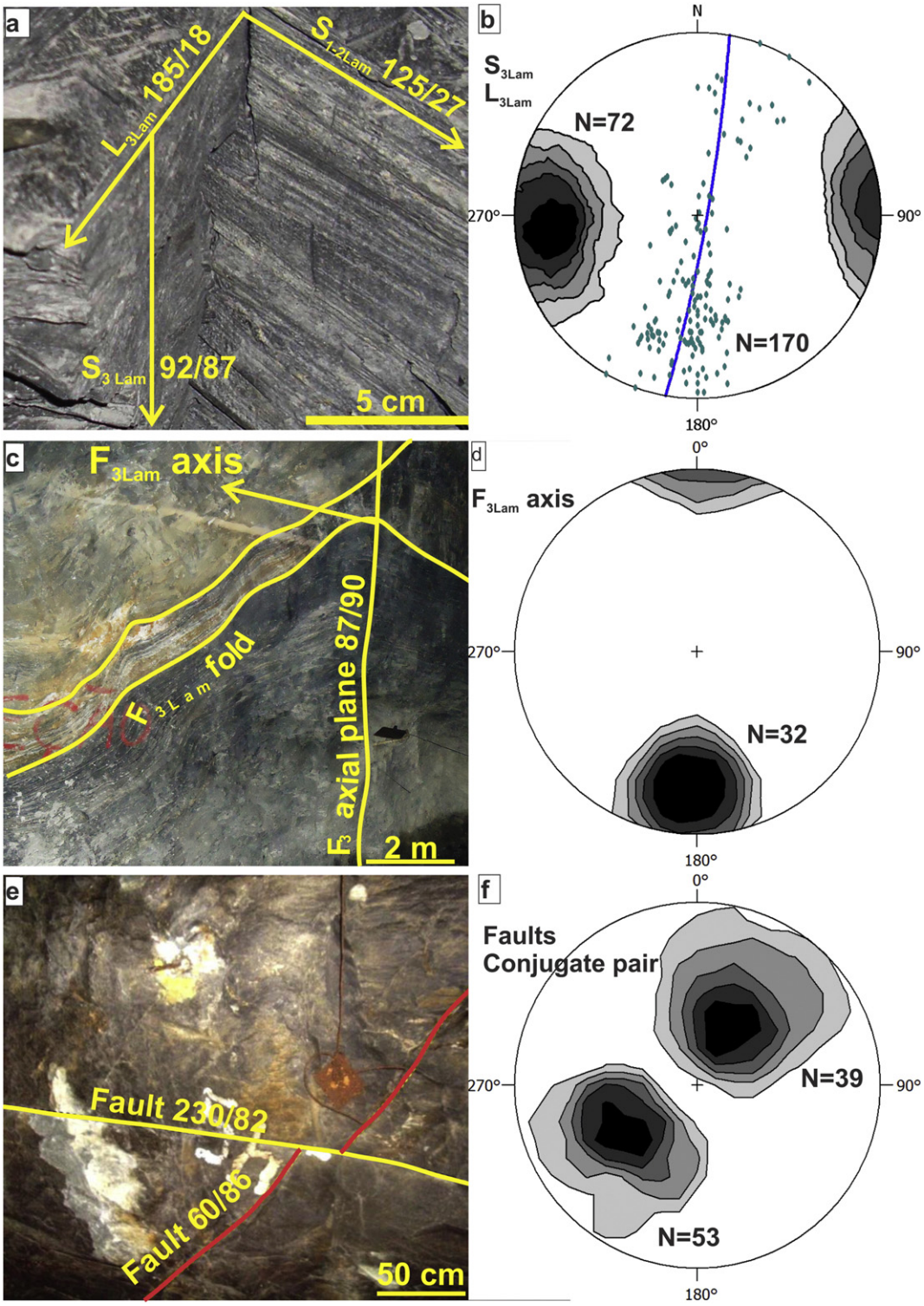


**Fig. 12.** Photo plates showing the relative timing of structural elements and stereographic projection that are displayed by density, equal-angle projection and lower hemisphere. (a) Geometrical relationship between $S_{1-2}$ and the vertical $S_3$ foliation that gave place to the formation of $L_3$; Arco da Velha orebody, level 1, Az. 15°. (b) The $S_3$ is oriented N–S/80°–90° and the $L_3$ in the N–S great circle has an average plunge of 70°. (c) $F_3$ folds develop in the carbonaceous pelites up to 3 m; Carruagem orebody, level 5.1, Az. 30°. (d) $F_3$ fold axes plunge 30° towards 180 to 200°. (e) Conjugate pair of faults developed as normal and reverse faults; Queimada orebody, level 1, Az. 315°. (f) Stereographic projection of fault pairs showing two distinct populations: one concentrated in the NE, and another in the SW.

### *9.3. Cambrian deformation event and the second (post-mineralization) structural generation — $G_2$: relationship to the $G_1$ structures*

The regional Cambrian deformation characterized as $D_4$ corresponds to the Brasiliano orogenic event (630–480 Ma; e.g., Pedrosa-Soares et al., 2011) that affected rocks of the Rio das Velhas and Minas Supergroups, with an E to W tectonic transport. This gave rise to N–S structures dipping to the E and W (Alkmim and Marshak, 1998; Baltazar and Zucchetti, 2007; Marshak and Alkmim, 1989).

At the deposit scale, the regional $D_4$ event is evidenced by the second structural generation — $G_2$, defined by the $S_3$ crenulation cleavage, which developed during the transposition of the $S_{1-2}$ foliation, and

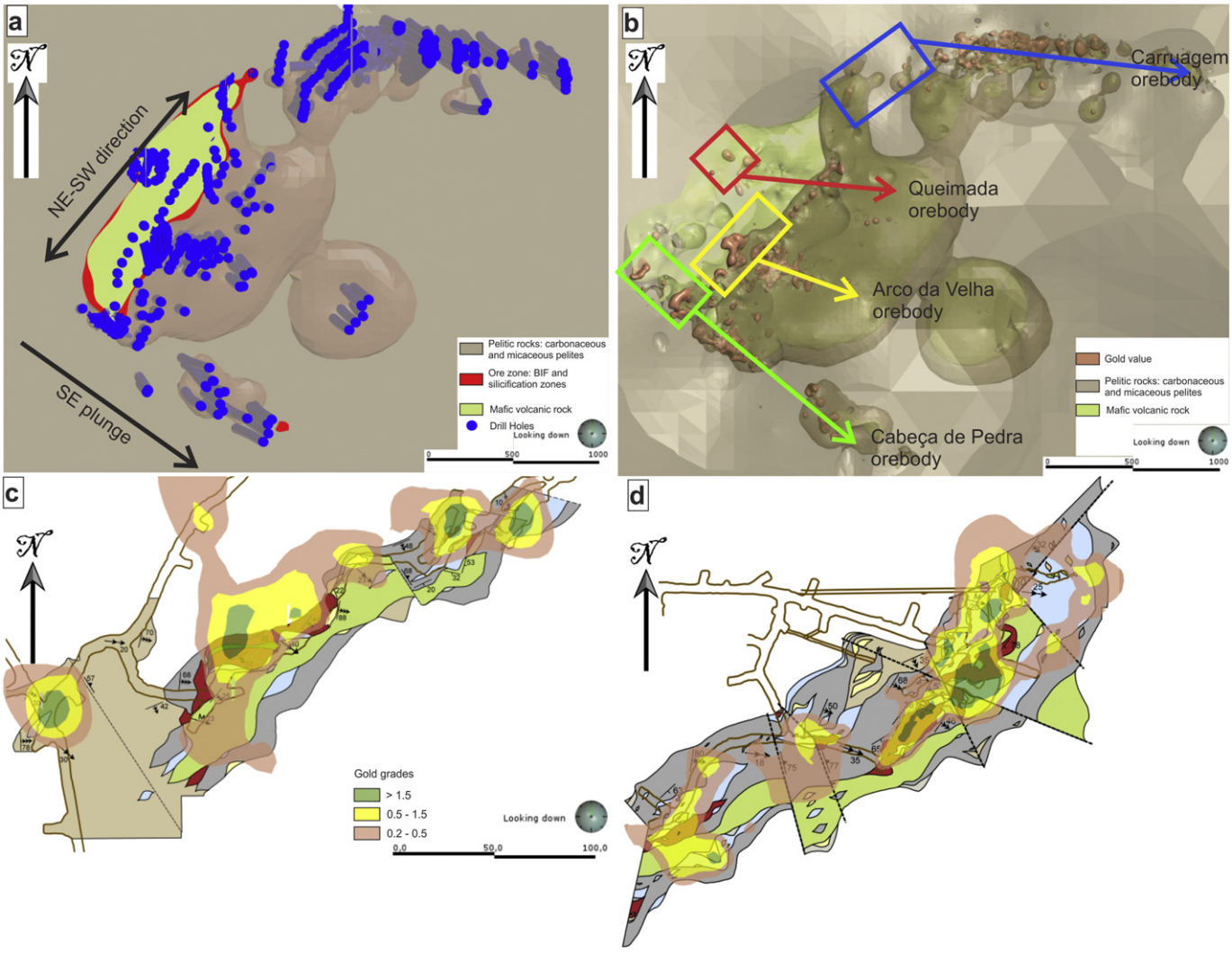


**Fig. 13.** (a) Outline marked by the footwall mafic and the hanging wall pelitic rocks that have both a general NE direction dipping to the SE. (b) Orebodies plunge according to legend of Fig. 8. Arrows follow the same color scheme as Fig. 8 for the Carruagem (blue), Queimada (red), Arco da Velha (yellow), and Cabeça de Pedra (green) orebodies. (c) Gold grades are represented as isosurfaces for the Carruagem orebody, level 1. (d) Idem, for Carruagem level 2.

therefore formed the intersection $L_3$ crenulation lineation and $F_3$ folds (Fig. 16d). The $F_3$ fold axes as well as the $L_3$ crenulation cleavage lineation are distributed along a great circle with an approximate N–S direction. The crenulation cleavage strikes NS and dips to the E (Lobato et al., 2013; Martins, 2011; Martins et al., 2011).

Two aspects that corroborate the Brasiliano orogenic event imprint on the Lamego gold deposit must be taken into consideration: (i) the direction and dip of the $G_2$ structures at Lamego are similar to the regional $D_4$ regional structures, defined as the Brasiliano orogenic event (Alkmim and Marshak, 1998; Baltazar and Zucchetti, 2007; Marshak and Alkmim, 1989), and (ii) the age of the hydrothermal xenotime at 518.5 ± 9 Ma (MSWD = 0.41; Table 3, Fig. 15c).

We interpret that the present position of the Lamego orebodies is due to their structural modification during the regional $D_4$ Brasiliano event.

## 10. Discussion

### *10.1. Evolution, age of mineralization and deformation events, and implications for the development of the Lamego orebodies*

The evolution at the Lamego deposit indicates that gold mineralization formed close to 2730 ± 42 Ma (MSWD = 0.51; Fig. 15b), based on new age data obtained from hydrothermal monazite grains associated with gold-bearing sulfides (Table 3, Fig. 15b). This is corroborated by the age of the Cuiabá and Morro Velho gold deposits at 2672 ± 14 Ma (MSWD = 2.3; Lobato et al., 2007), although the latter study did not detect younger Proterozoic ages. This is also in tune with the long-standing notion of NE–SW compression resulting in NW–SE-trending structures as being of Archean age.

The discordant 2387 ± 46 Ma age on hydrothermal monazite, developed along $S_{1-2}$ (Fig. 15b), is interpreted with much caution, since it was obtained with two discordant (13% disagreement) monazite grains. The importance or significance of this age for gold mineralization at the Lamego deposit with respect to the regional context is not yet fully understood.

The Minas Supergroup is an 8 km-thick passive-margin to syn-orogenic sedimentary package (Alkmim and Noce, 2006), deposited between ~2.5 and 2.12 Ga (Alkmim and Marshak, 1998; Dorr, 1969; Hartmann et al., 2006; Machado and Carneiro, 1992), and deformed during the Rhyacian. The Paleoproterozoic TTG suites of the QF region and surroundings are usually dated between 2.2 and 2.1 Ga (e.g., Almeida, 2000).

In a recent contribution, Teixeira et al. (2015) obtained a LA–ICPMS U–Pb zircon age of 2351 ± 48 Ma for the tholeiite-sourced Resende Costa orthogneiss suite in the Mineiro belt, some 190 km SW of the

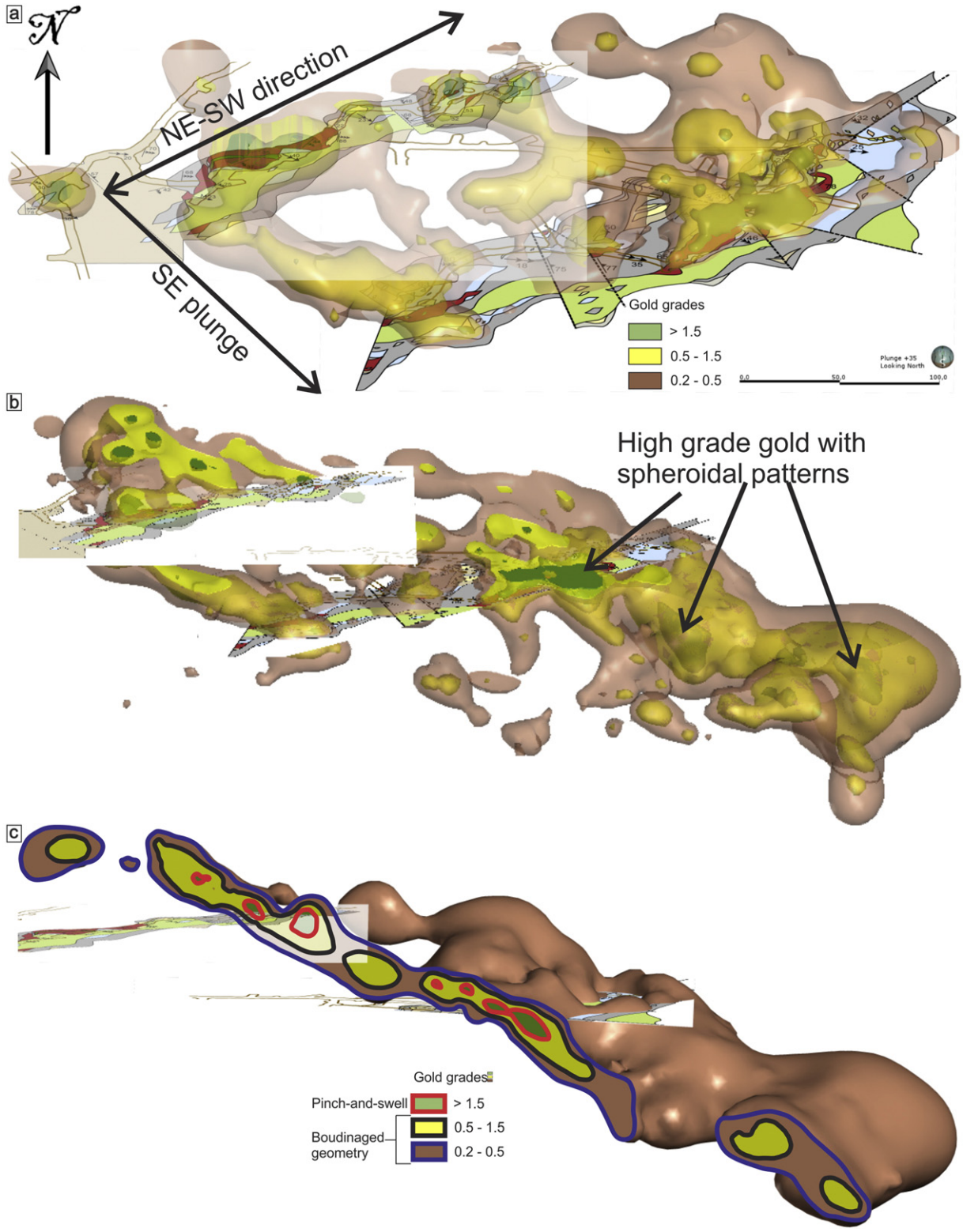


**Fig. 14.** (a) Section through the Carruagem orebody showing the mineralization sub-parallel to parallel to the $S_{1-2}$ foliation. (b) Sections cutting parallel to the $S_{1-2}$ foliation, with the high-grade gold lenses exhibiting a spheroidal pattern. (c) Sections cutting perpendicular to the $S_{1-2}$ foliation show a boudinaged geometry that evolves into pinch-and-swell.

Lamego deposit. Seixas et al. (2012) dated the high-aluminum Lagoa Dourada TTG suite, in the same belt, at 2350 Ma (zircon, U–Pb ID–TIMS). These data led Teixeira et al. (2015) to suggest that both the Resende Costa–Lagoa Dourada rocks characterize the precocious arc magmatism of the Minas accretionary orogeny, which would have lasted some 350 Ma.

The 2387 ± 46 Ma age (Fig. 15b) may be related to the early stages of the Minas accretionary orogeny of Teixeira et al. (2015), and represent the imprint on the Rio das Velhas greenstone belt, which affected the Lamego deposit area. Despite this possible mineral growth at 2387 ± 46 Ma, the Paleoproterozoic regional $D_3$ gave place to a weakly developed foliation (Alkmim and Marshak,

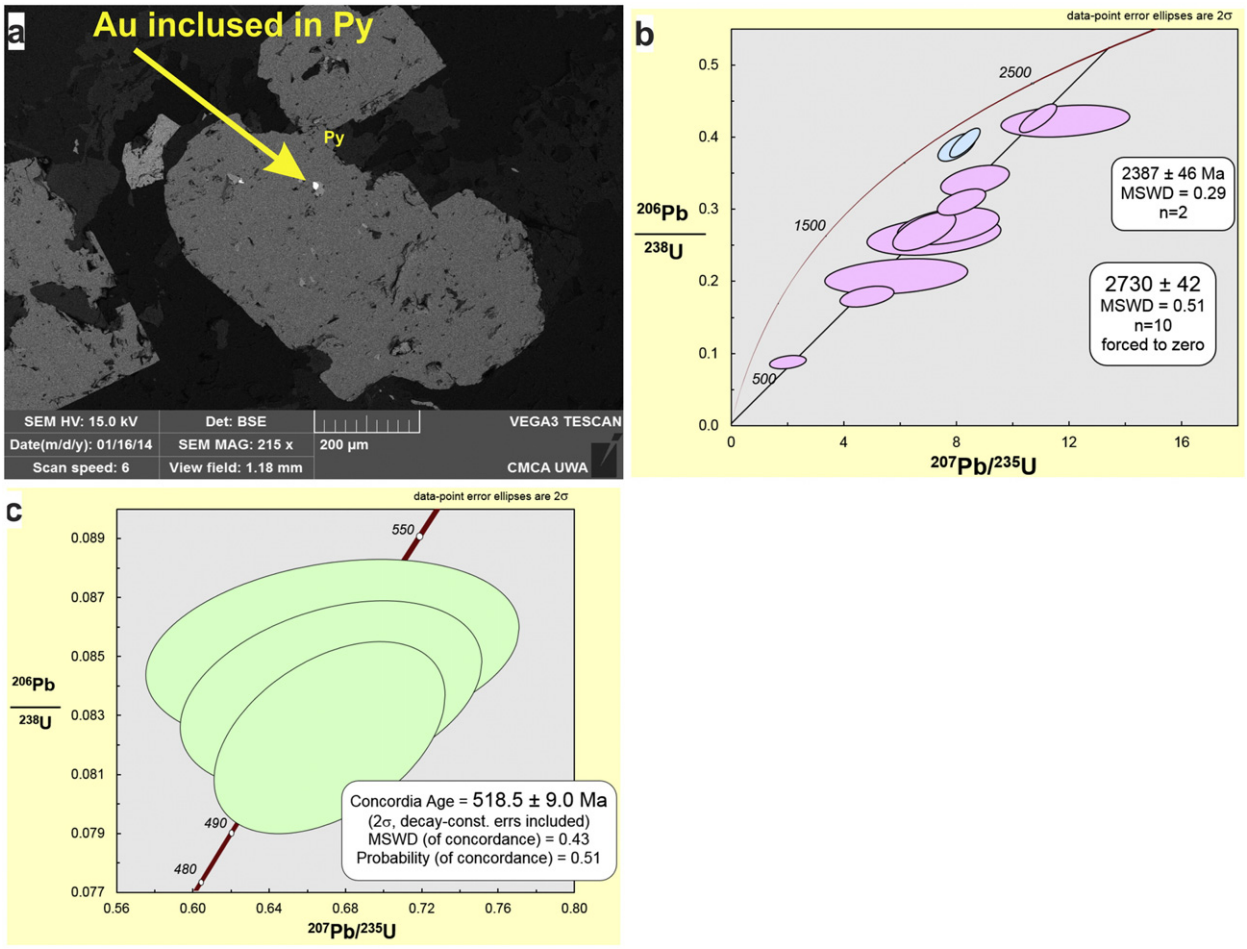


**Fig. 15.** Image of back-scattered electrons and concordia diagrams of mafic volcanic rock (mineralized sericite–quartz–carbonate ± chlorite ± pyrite schist; LM-CP), selected for geochronological studies at the Lamego deposit (data in Table 3); Cabeça de Pedra orebody, level 3. (a) Representative back-scattered electron images of sulfide crystals showing gold grain included in pyrite. (b) Concordia plot of SHRIMP U–Pb data for hydrothermal monazite. The weighted mean $^{207}Pb/^{206}Pb$ age of the main concordant cluster is 2730 ± 42 Ma (2 sigma; MSWD = 0.51). Two monazites are discordant, younger at 2387 ± 46 Ma. (c) Concordia plot of SHRIMP U–Pb data for hydrothermal xenotime. The weighted mean $^{207}Pb/^{206}Pb$ age of the main concordant cluster is 518.5 ± 9 Ma (MSWD = 0.41; 2 sigma).

1998), which was not defined at the mine site, or conceivably, parallelized to $S_{1-2}$.

Goldfarb and Groves (2001) indicate two major episodes of orogenic gold deposit formation in the Precambrian, during the intervals from 2800 to 2550 Ma and from 2100 to 1800 Ma. Despite the monazite age at 2387 ± 46 Ma, it is difficult to envisage the Archean gold mineralization remobilized at this time. As pointed out by Fyfe (1987), remobilization of ore deposits is improbable, unless large fluid volumes are involved, or the crust undergoes major tectonic re-arrangement. For the most part, remobilization of existing ores must take place via interaction of new fluids; the chemical environment associated with the influx of new fluids must differ from that associated with deposition, otherwise new transfer processes would not operate (Hobbs, 1987). Wilkinson et al. (1999, and references therein) discuss $H_2O$–$CO_2$–NaCl-dominated fluids in orogenic gold systems, and indicate that low-temperature, high-salinity brines may be interpreted as a product of late-stage phase separation, or as overprinting fluids that reset isotopic systematics and introduce new mineral phases. However, the genetic relationship, if any, between such brines and gold mineralization has proven difficult to establish (Wilkinson et al., 1999).

It is also interesting to note that De Witt et al. (2000) and Thorper et al. (1984) documented a Paleoproterozoic isotopic disturbance on some Rio das Velhas greenstone-belt-hosted gold deposits using Pb–Pb model ages.

Xenotime crystals yielded a 518.5 ± 9 Ma age (Table 3, Fig. 15c), which reveals the strong imprint of the Brasiliano orogenic event recognized in the QF region by many authors (e.g., Alkmim and Marshak, 1998; Baltazar and Zucchetti, 2007; Table 1).

The Brasiliano event in the Araçuaí orogen, in the eastern portion of the São Francisco Craton, is established at the range of 0.630 and 0.480 Ga, based on a succession of five granitic events $G_1$ to $G_5$ (Pedrosa-Soares et al., 2011). In this orogen, there is one region that is known as the N–S-trending Eastern Brazilian Pegmatite Province, where these granitic events are associated with $G_4$ and $G_5$ granites (Pedrosa-Soares et al., 2011). The 518.5 ± 9 Ma xenotime age falls in the $G_4$ super suite time of formation (535 to 500 Ma), somewhat in transition to the $G_5$ (520 to 480 Ma). Pegmatites associated with the Brasiliano event are also intruded in rocks of the Minas Supergroup, as is the case of the Piracicaba Group, about 140 km east of Lamego, where a Rb–Sr date of 545 Ma was obtained on amazonite (Herz,

**Fig. 16.** Schematic cartoon structural model without scale for the formation of the Lamego gold deposit. (a) The lithologies are folded and shear zones started to develop; (b) As shear zones progressed, veins evolved and both functioned as pathways for hydrothermal fluids, which precipitated coarse-grained, irregular zones of smoky quartz in massive veins. These veins were progressively deformed, assumed the structural aspect of boudins, and as their recrystallization advanced, fine-grained milky quartz formed. Gold mineralization generally coincides with the development of pyrite and As-rich pyrite, sulfide zones. (c) Refolding of the Lamego structure as part of the $D_1$–$D_2$ progressive event. (d) Final stage of the Lamego gold deposit evolution with the modification of the orebodies in the Cambrian probably as a result of the late stages of the Brasiliano orogeny (see text for explanation).

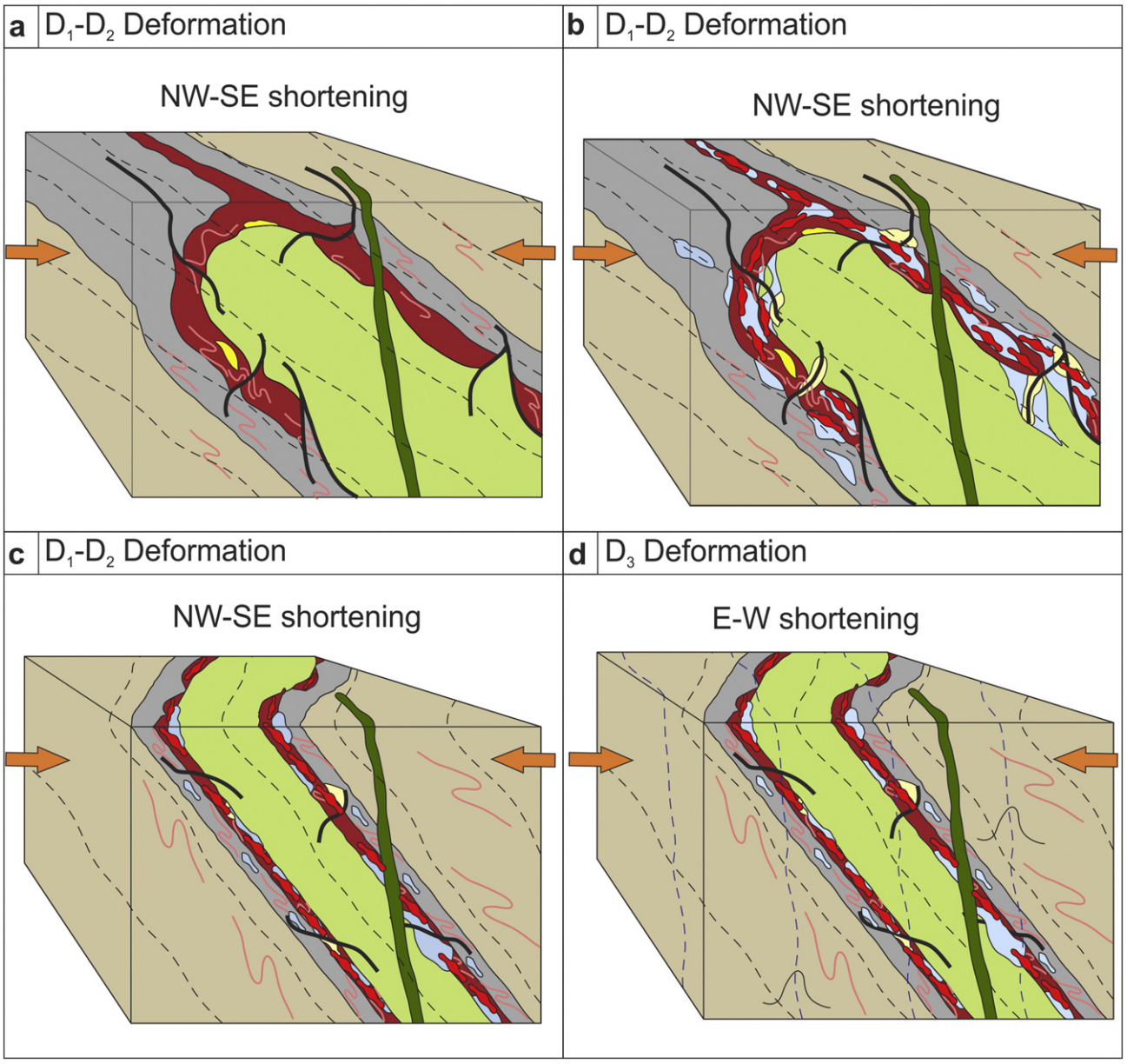


Diabase dike
Micaceous pelite
Carbonaceous pelite
Banded iron formation
(Including chert-rich horizons)
Mafic volcanic rocks (basalts)

Silicification zones
Milky quartz
Late $D_2$ event
Smoky qhuartz
$D_2$ event, locally
boudins or veins

**$D_1$-$D_2$ Structures**
Contact
Thrust fault
$S_{1-2}$ foliation, parallel to $F_2$ fold
$F_2$ fold
Sulfide(Py)-rich gold mineralization (> 2.5 g/t Au)

**$D_3$ Structures**
$S_3$ Foliation, crenulation cleavage parallel to local fold
$F_3$ fold

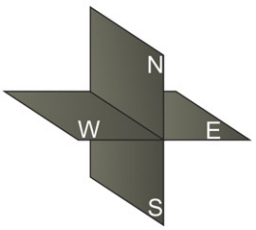

1970). The author considers this to be the result of a thermal, magmatic event about 500 Ma ago. We suggest that the 518.5 ± 9 Ma xenotime age records the (i) N–S-trending $G_2$ post-mineralization structures and the regional $D_4$, linked to the regional E–W shortening, and the (ii) Brasiliano thermal magmatic event that is locally expressed by the presence of pegmatites, which intrude the Minas Supergroup that in turn overlies and variably deforms the Rio das Velhas Supergroup.

### *10.2. Comparison with other Archean orogenic gold deposits in Brazil and worldwide*

Orogenic gold deposits in Archean greenstone belt terrains are recognized as major gold producers. Examples include deposits located in the Yilgarn craton of Western Australia and the Superior province of Canada (Goldfarb et al., 2005; Goldfarb and Groves, 2001; Groves et al., 2003, 1998; Hagemann and Cassidy, 2000; Robert et al., 2005). In both examples, the gold deposits are: (i) related to collision tectonic environments, (ii) controlled by structures such as fault systems, shear zones and folds, (iii) hosted by a variety of rocks including volcanic–sedimentary, such as BIF, and granites, and (iv) associated with hydrothermal alteration, with pyrite, arsenopyrite and pyrrhotite being the main sulfide minerals.

Orogenic gold deposits in the Rio das Velhas greenstone belt (e.g., Lobato et al., 2001a; Vial et al., 2007a) show similarities with other Archean BIF-hosted deposits around the world. They are confined by Fe-rich portions of the BIF These portions are structurally controlled by shear zones and folds, and plunge consistently to the SE, as is the case at Lamego, Cuiabá and Morro Velho. They contain gold associated with pyrrhotite, pyrite and arsenopyrite (e.g., Raposos — Junqueira et al., 2007; São Bento —Martins Pereira et al., 2007; Cuiabá —Ribeiro-Rodrigues et al., 2007; Morro Velho —Vial et al., 2007b; Fig. 1). Geological characteristics at Lamego that are compatible with BIF-hosted orogenic gold deposits around the world are: (i) mineralization structurally controlled and associated with crustal compression, defined by the $G_1$ structures as $F_2$ folds, boudins and shear zones; (ii) structural controls of orebodies associated with $F_2$ fold axis and $L_{1-2}$ lineations plunging to the SE; (iii) high-gold grades confined to Fe-rich host lithologies and silicification zones; (iv) silicification, sulfidation and carbonatization as the major hydrothermal alteration processes in the mineralized zones, and (v) three styles of gold mineralization including vein, replacement and disseminated.

The Lamego deposit also displays differences when compare to other BIF-hosted deposits in the Rio das Velhas greenstone belt. These include individual orebodies in the Lamego deposit that show different plunge directions. For example, the Cabeça de Pedra orebody plunges 25 towards 130, and the Carruagem orebody plunges 22 towards 95, here interpreted as a structural modification imposed by the Brasiliano tectonic cycle, which had a particularly strong effect on the Lamego orebodies.

That opens the possibility that other BIF-hosted gold deposits in the QF display more than one plunge direction. Further detailed structural analysis combined with gold grade distribution need to be applied to test this possibility. Such analysis associated with high-precision geochronology can provide a good insight on the tectonic evolution of the deposit.

### *10.3. Implications for exploration in the QF*

The combined structural and geochronological analysis of the Lamego deposit provides significant constrains to the targeting of the orogenic gold systems in the Archean terrain of the QF. At least three important observations can be summarized from the structural lithological mapping of the Lamego deposit.

Firstly, in the volcanic–sedimentary rock package hosting the Lamego gold deposit the carbonaceous pelites are the primary lithological exploration target. That is because the carbonaceous pelites acted as a seal whereby the gold-bearing hydrothermal fluids stopped at the contact with BIF-carbonaceous pelites. These contact zones display the highest grade in the entire Lamego gold deposit. Furthermore, they also contain the high-gold grade silicification zones that represent one significant mineralization style at Lamego.

Secondly, the main structural exploration targets in the Lamego area, NW portion of QF, are the NW–SE plunging, $F_2$ reclined folds. That is the case because the hinge zones of these folds represent the highest-grade gold ore zones in the Lamego deposit.

Thirdly, the regional $D_4$ Brasiliano event — related with normal fault zones and crenulation cleavage — affected the entire QF (Fig. 1). In the Lamego deposit, these structures can also be observed and have resulted in significant modification of the established orebodies (Fig. 3a, b, c). The modification includes lateral offset of the ore shoots, thinning of ore zones and decrease in gold contents. Importantly, the orebodies are not cut off, and they continue below the areas affected by regional $D_4$ Brasiliano-related structures (Figs. 11 and 12). That poses the question of whether the deposits interrupted by these younger structures, as for the São Bento deposit (Fig. 1), indeed continue below them. The targeting of the extension of orebodies below these structures has to be considered during drilling campaigns.

## 11. Conclusions

The detailed lithological and structural geological mapping of several orebodies at different mine levels, structural analysis and indirect and implicit 3D orebody modeling at the Lamego gold deposit, with special emphasis on the Carruagem orebody, combined with high-precision U–Pb geochronology, reveal the following conclusions:

(1) From bottom to top the lithostratigraphy at the Lamego deposit is defined by mafic volcanic rock, a metabasalt (chlorite–carbonate–sericite–quartz schist); banded chert with BIF that is both carbonaceous and/or ferruginous; and carbonaceous and micaceous pelites (Fig. 2). These all contain metamorphic index minerals (sericite–chlorite–quartz–carbonate), which are indicative of greenschist facies metamorphism.
(2) Both chert and BIF bands are referred to as the Lamego BIF. The bands of the Lamego BIF are characterized by alternating dark carbonate–quartz (± magnetite) and light quartz–carbonate bands (Fig. 6c, d).
(3) Pelitic rocks are represented by carbonaceous and micaceous pelites (Fig. 6g, h), and they envelop the entire Lamego deposit.
(4) The macrostructure Lamego fold is defined as a rootless, reclined, isoclinal, cylindrical fold with a NE–SW striking axial plane, dipping 30° to the SE (map in Fig. 3a). The fold hinge zone in the SW quadrant is represented by the Cabeça de Pedra orebody (Fig. 3b); the normal limb (SE quadrant) is the Arco da Velha orebody (Fig. 3c); the overturned limb (SE quadrant) is the Queimada orebody (Fig. 3c); and the limb intersection (NE quadrant) is the Carruagem orebody.
(5) Two structural generations, $G_1$ and $G_2$, are recognized at the Lamego deposit (Table 5). The $G_1$ structures are represented by: (i) the planar structures' $S_{1-2}$ foliation, $V_1$ and $V_2$ veins, and shear zones; these are generally oriented NE–SW, dip to the SE, with the exception of $V_1$ veins that dip to the NE and probably represent the oldest structures at the Lamego deposit; and (ii) the linear structures' $L_{1-2}$ lineation and $F_2$ fold axis that plunge to the SE. The $G_2$ structures are represented by: (i) the N–S oriented $S_3$ crenulation cleavage, dipping to the E; and (ii) the $F_3$ fold axis and $L_3$ crenulation lineation that are N–S oriented and plunge to the S.
(6) Since the regional Paleoproterozoic $D_3$ foliation is not clearly recognized at the Lamego deposit, and its regional trend is similar to both $S_0$ and $S_{1-2}$, it is likely that this regional foliation overprinted the $S_{1-2}$ and, therefore, both are indistinguishable.
(7) The $S_3$ spaced/crenulation cleavage is related to the regional $D_4$ Brasiliano N–S-trending regional folds and thrusts, with vergence to the E. These regional $D_4$ folds moved the $G_1$ structures to their

current position; the $G_1$ structures had an original NW–SE direction, which was probably the trend of the Rio das Velhas Archean belt.

(8) The main hydrothermal alteration minerals are quartz, pyrite, arsenopyrite and pyrrhotite, and they are developed parallel to the $S_{1-2}$ foliation in all rock types.

(9) The quartz-rich (silicification) zone is characterized by three quartz types: (i) deformed, coarse-grained smoky quartz that occurs as irregular masses, both concordant and discordant, within the mineralized zones; (ii) fine-grained, granoblastic, white and milky quartz formed from the recrystallization of smoky quartz; and (iii) milky quartz, particularly in fault zones cutting across (i) and (ii) types.

(10) Three styles of gold mineralization are identified at the Lamego deposit, namely vein, replacement and disseminated styles. The Lamego mineralization is mainly hosted by a sulfide-associated, replacement style.

(11) High-grade gold lenses (Figs. 13c, d and 14a) show a spheroidal pattern and a distribution that varies along the $S_{1-2}$ foliation. These lenses represent the hinge zone of $F_2$ reclined folds with the plunge of the orebodies controlled by the $F_2$ fold axes.

(12) The lower-grade gold lenses are controlled by pinch and swell, and locally expressed quartz boudins. The latter have two orthogonal directions, one to the NW–SE and the other to the NE–SW, thereby defining chocolate-tablet style boudinage.

(13) The hydrothermal monazite age of 2730 ± 42 Ma (2 sigma; MSWD = 0.51; Fig. 15b) is interpreted to represent the age of gold mineralization synchronous to the $G_1$ structures.

(14) Though discordant, the 2387 ± 46 Ma age obtained on hydrothermal monazite (Fig. 15b) may be interpreted as relating to the early stages of the Minas accretionary orogeny, and represents the structural imprint on the Rio das Velhas greenstone belt, which affected the Lamego deposit area. Despite this monazite age, it is difficult to envisage the Archean gold mineralization remobilized at this time, since remobilization of gold deposits would require very large fluid volumes, which cannot be clearly established for Lamego.

(15) The xenotime age of 518.5 ± 9 Ma (MSWD = 0.41; 2 sigma) is interpreted as the strong imprint of the Brasiliano orogenic event in the QF region, which is reflected by: (i) the N–S-trending $G_2$ structural generation post-mineralization deformation and the regional $D_4$ structures, linked to the regional E–W shortening, and (ii) an important Brasiliano thermal, magmatic event described in the Araçuaí orogen, expressed locally by the presence of pegmatites intruding the Minas Supergroup that overlies the Rio das Velhas Supergroup.

(16) Although the Brasiliano-age deformation, which was responsible for the development of the $G_2$ structures, dislocated the orebodies in the Lamego mine, there is no evidence for the formation of new hydrothermal alteration minerals, sulfides and gold. There is also no evidence for any recrystallization of the Archean hydrothermal alteration zones or mineralized areas including sulfides and gold.

(17) Development of exploration targeting criteria for the preferred location of gold in BIF-hosted orogenic gold deposit in the QF and partially worldwide include: (i) carbonaceous pelites along the contact with BIF, and (ii) $F_2$ reclined folds.

(18) The regional $D_4$-type structures that affect the Lamego's orebodies need to be considered for the exploration criteria since this caused the modification of a Lamego Archean orogenic gold deposit.

## Acknowledgments

This research is the result of the on-going Ph. D. thesis by the first author at the Federal University of Minas Gerais — UFMG, which is fully financed by Brazil's National Council of Technological and Scientific Development — CNPq, Vale and AngloGold Ashanti Córrego do Sítio Mineração S/A-AGA. The student's scholarship is granted by CNPq. LML and CAR also acknowledge grants from the CNPq.

The authors thank AGA for their logistic and technical support, and for allowing the publication of this manuscript. Special thanks are due to Rodrigo Martins who has maintained his commitment to our research group throughout. We are indebted to present and past colleagues at the Lamego mine, especially Jorge Watanabe, for the many technical debates and mine visits. Discussions with Orivaldo Baltazar from the CPRM-Brazil's Geological Survey over the regional overviews were fundamental. We also acknowledge the support of UFMG, UWA, CAPES, FAPEMIG and FUNDEP. Special thanks to Bruna Ketlyn Silva Cota who helped draw the pictures, images and tables; Geoffrey Batt who granted the Leapfrog Geo license used for making the 3D model, geologist Polyane Figueiredo for the collaboration in the discussion about the 3D geological model, and Marcelo Freitas of Aranz Geo, for granting us with an academic Leapfrog license.

## References

Alkmim, F.F., Marshak, S., 1998. Transamazonian orogeny in the Southern Sao Francisco craton region, Minas Gerais, Brazil: evidence for Paleoproterozoic collision and collapse in the Quadrilátero Ferrífero. Precambrian Res. 90, 29–58.

Alkmim, F.F., Noce, C., 2006. The Paleoproterozoic record of the São Franscisco Craton. IGCP 509 Field workshop, Bahia and Minas Gerais, Brazil. Field Guide & Abstracts, Brazil, p. 114.

Almeida, F.F.M., 1977. O Cráton do São Francisco. Rev. Bras. Geosci. 7, 349–364.

Almeida, F.F.M., de Brito Neves, B.B., Dal Ré Carneiro, C., 2000. The origin and evolution of the South American Platform. Earth Sci. Rev. 50, 77–111.

Baltazar, O.F., Pedreira, A.J., 1998. In: Departamento Nacional de Produção Mineral. Associações litofaciológicas. (Belo Horizonte), DNPM.

Baltazar OF, Silva SL. Relatório Mapa Geológico Integrado do Supergrupo Rio das Velhas, escala 1:100.000. In: Mineral DNPM, editor. Belo Horizonte: Departamento Nacional de Produção Mineral; 1996. p. 136.

Baltazar, O.F., Zucchetti, M., 2007. Lithofacies associations and structural evolution of the Archean Rio das Velhas greenstone belt, Quadrilátero Ferrífero, Brazil: a review of the setting of gold deposits. Ore Geol. Rev. 32, 471–499.

Bierlein, F.P., Groves, D.I., Goldfarb, R.J., Dubé, B., 2006. Lithospheric controls on the formation of provinces hosting giant orogenic gold deposits. Mineral. Deposita 40, 874–886.

Brandt, R.T., Gross, G.A., 1972. Problems of nomenclature for banded ferruginous–cherty sedimentary rocks and their metamorphic equivalents. Econ. Geol. 67, 682–684.

Brito Neves, B.B., 2011. The Paleoproterozoic in the South-American continent: diversity in the geologic time. J. S. Am. Earth Sci. 32, 270–286.

Carneiro, M.A., Teixeira, W., Machado, N., 1994. Geological evolution of a sialic Archaean crustal fragment from the Quadrilátero Ferrífero in eastern-central Brazil, based on U–Pb, Sm–Nd, Rb–Sr, and K–Ar isotopic constraints. Terra Noxtra 2, 12–13.

Davis, G.H., Reynolds, S.J., 1996. Structural Geology of Rocks and Regions. John Wiley, New York.

De Witt, E., Thorman, C., Ladeira, E., Zartman, R., Landis, G., Wooden, J., 2000. Origin and age of gold deposits at São Bento and Morro Velho, Brazil. 31th International Geological Congress, Rio de Janeiro, Brazil, CD-ROM.

Dorr, J.V.N., 1957. In: Mineral DNPM (Ed.), Revisão da Estratigrafia Pré-cambriana do Quadrilátero Ferrífero: Brasil. Departamento Nacional de Produção Mineral, Minas Gerais, p. 81.

Dorr, J.V.N., 1969. Physiographic, Stratigraphic and Structural Development of the Quadrilátero Ferrífero, Minas Gerais, Brazil. Regional Geology of the Quadrilátero Ferrífero, Minas Gerais, Brazil.

Fletcher, I.R., McNaughton, N.J., Aleinikoff, J.A., Rasmussen, B., Kamo, S.L., 2004. Improved calibration procedures and new standards for U–Pb and Th–Pb dating of Phanerozoic xenotime by ion microprobe. Chem. Geol. 209, 295–314.

Fletcher, I.R., McNaughton, N.J., Davis, W.J., Rasmussen, B., 2010. Matrix effects and calibration limitations in ion probe U–Pb and Th–Pb dating of monazite. Chem. Geol. 270, 31–44.

Foster, G., Kinny, P., Vance, D., Prince, C., Harris, N., 2000. The significance of monazite U–Th–Pb age data in metamorphic assemblages; a combined study of monazite and garnet chronometry. Earth Planet. Sci. Lett. 181, 327–340.

Fyfe, W.S., 1987. Tectonics, fluids and ore deposits: mobilization and remobilization. Ore Geol. Rev. 2, 21–36.

Gair, J.E., 1962. Geology and Ore Deposits of the Nova Lima and Rio Acima Quadrangles. US Government Printing Office, Minas Gerais, Brazil.

Goldfarb, R., Groves, D., 2001. Orogenic gold and geologic time: a global synthesis. Ore Geol. Rev. 18, 1–75.

Goldfarb, R.J., Baker, T., Dubé, B., Groves, D.I., Hart, C.J., Gosselin, P., 2005. Distribution, character, and genesis of gold deposits in metamorphic terranes. Economic Geology 100th Anniversary Volume, pp. 407–450.

Gross, G.A., 1965. Geology of Iron Deposits in Canada. Department of Mines and Technical Surveys, Canada.

Gross, G.A., 1980. A classification of iron formations based on depositional environments. Can. Mineral. 18, 215–222.

Groves, D.I., Goldfarb, R.J., Gebre-Mariam, M., Hagemann, S., Robert, F., 1998. Orogenic gold deposits: a proposed classification in the context of their crustal distribution and relationship to other gold deposit types. Ore Geol. Rev. 13, 7–27.
Groves, D.I., Goldfarb, R.J., Robert, F., Hart, C.J., 2003. Gold deposits in metamorphic belts: overview of current understanding, outstanding problems, future research, and exploration significance. Econ. Geol. 98, 1–29.
Hagemann, S., Cassidy, K.F., 2000. Archean orogenic lode gold deposits. Gold in 2000, pp. 9–68.
Hagemann, S., Gill, H.A., 2011. Oxygen and hydrogen isotope study of the archean granulite-hosted Griffin's Find gold deposit, Western Australia. In: Reich, M., Barra, F., Tornos, F. (Eds.), Let's Talk Ore Deposits Proceedings of 11th Biennial SGA Meeting. Antofagasta, Chile.
Hartmann, L.A., Endo, I., Suita, M.T.F., Santos, J.O.S., Frantz, J.C., Carneiro, M.A., et al., 2006. Provenance and age delimitation of Quadrilátero Ferrífero sandstones based on zircon U–Pb isotopes. Journal of South American Earth Sciences. 20, 273–285.
Herz, N., 1970. Gneissic and Igneous Rocks of the Quadrilátero Ferrífero. US Government Printing Office, Minas Gerais, Brazil.
Hill, E.J., Oliver, N.H., Cleverley, J.S., Nugus, M.J., Carswell, J., Clark, F., 2013. Characterisation and 3D Modelling of a Nugget, Vein-hosted Gold Orebody, Sunrise Dam, Western Australia.
Hill, E., Oliver, N.H., Fisher, L., Cleverley, J.S., Nugus, M.J., 2014. Using Geochemical Proxies to Model Nuggety Gold Deposits: An Example from Sunrise Dam, Western Australia.
Hobbs, B.E., 1987. Principles involved in mobilization and remobilization. Ore Geol. Rev. 2, 37–45.
James, H.L., 1954. Sedimentary facies of iron-formation. Econ. Geol. 49, 235–293.
Junqueira, P., Lobato, L., Ladeira, E., Simões, E., 2007. Structural control and hydrothermal alteration at the BIF-hosted Raposos lode-gold deposit, Quadrilátero Ferrífero Brazil. Ore Geol. Rev. 32, 629–650.
Kerrich, R., Goldfarb, R.J., Groves, D.I., Garwin, S., 2000. The Geodynamics of World-class Gold Deposits: Characteristics, Space–Time Distribution, and Origins. Reviews in Economic Geology. Society of Economic Geologist, Boulder, Colorado, pp. 501–551.
Kerrich, R., Goldfarb, R.J., Richards, J.P., 2005. Metallogenic provinces in an evolving geodynamic framework. Econ. Geol. 100, 1097–1136.
Ladeira, E., 1980a. Geology, petrography and geochemistry of Nova Lima Group, Quadrilátero Ferrífero, Minas Gerais, Brasil. XVII Geowiss Lateinamer. Heidelberg, pp. 47–48.
Ladeira, E., 1980b. Gênese do Ouro na Mina de Morro Velho e no Distrito de Nova Lima, Minas Gerais, Brasil. In: Geologia SBd (Ed.), 31° Congresso Brasileiro de Geologia. Sociedade Brasileira de Geologia, Camboriu, p. 371.
Lana, C., Alkmim, F.F., Armstrong, R., Scholz, R., Romano, R., Nalini Jr., H.A., 2013. The ancestry and magmatic evolution of Archaean TTG rocks of the Quadrilátero Ferrífero province, southeast Brazil. Precambrian Res. 231, 157–173.
Lima, T.M., CAR, N., 2014. In: Mineral DNdP (Ed.), Sumário Mineral 2014. Ministério de Minas e Energia, Brasília, Distrito Federal, p. 148.
Lobato, L.M., Vieira, F.W.R., 1998a. Styles of hydrothermal alteration and gold mineralization associated with the Nova Lima Supergroup of the Quadrilátero Ferrífero: Parte I, Description of selected gold deposit. Rev. Bras. Geosci. 28, 339–354.
Lobato, L.M., Vieira, F.W.R., 1998b. Styles of hydrothermal alteration and gold mineralization associated with the Nova Lima Supergroup of the Quadrilátero Ferrífero: Parte II, The Archean mesothermal gold-bearing hydrothermal system. Rev. Bras. Geosci. 28, 355–366.
Lobato, L.M., Ribeiro-Rodrigues, L.C., Vieira, F.W.R., 2001b. Brazil's premier gold province. Part II: Geology and genesis of gold deposits in the Archean Rio das Velhas greenstone belt, Quadrilátero Ferrífero. Mineral. Deposita 36, 249–277.
Lobato, L.M., Ribeiro-Rodrigues, L.C., Zucchetti, M., Noce, C.M., Baltazar, O.F., da Silva, L.C., et al., 2001a. Brazil's premier gold province. Part I: The tectonic, magmatic and structural setting of the Archean Rio das Velhas greenstone belt, Quadrilátero Ferrífero. Mineral. Deposita 36, 228–248.
Lobato LM, Martins BdS, Rosière CA, Figueiredo e Figueiredo e Silva RC, Lemos LHA, Villanova FLSP, et al. Depth variation characteristics at the Carruagem orebody, Archean BIF-hosted Lamego gold deposit, Quadrilátero Ferrífero, Brazil. In: Applied SG, editor. 12th SGA Biennial Meeting — Mineral Deposit Research for a High-Tech World. Uppsala, Sweden: SGA; 2013. p. 1144–1147.
Lobato, L., Santos, J., McNaughton, N., Fletcher, I., Noce, C., 2007. U–Pb SHRIMP monazite ages of the giant Morro Velho and Cuiabá gold deposits, Rio das Velhas greenstone belt, Quadrilátero Ferrífero, Minas Gerais, Brazil. Ore Geol. Rev. 32, 674–680.
Ludwig, K.R., 2003. User's Manual for Isoplot 3.00: A Geochronological Toolkit for Microsoft Excel. Kenneth R. Ludwig.
Ludwig, K., 2009. SQUID 2: A User's Manual 100. Berkeley Geochronology Center.
Machado, N., Carneiro, M.A., 1992. U–Pb evidence of Late Archean tectonothermal activity in the southern São Francisco shield, Brazil. Can. J. Earth Sci. 29, 2341–2346.
Machado N, Noce CM, Oliveira OAB, Ladeira EA. Evolução Geológica do Quadrilátero Ferrífero no Arqueano e Proterozóico Inferior com Base em Geogronologia U–Pb. In: Geologia SBd, editor. Anais do V Simpósio de Geologia de Minas Gerais. Belo Horizonte: Núcleo Minas Gerais; 1989. p. 1–4.
Marshak, S., Alkmim, F.F., 1989. Proterozoic contraction/extension tectonics of the southern São Francisco region, Minas Gerais, Brazil. Tectonics 8, 555–571.
Martins, B.S., 2011. Controle da Mineralização Aurífera de Lamego, Sabará, Quadrilátero Ferrífero, MG. [Master Degree. Universidade de Minas Gerais, Belo Horizonte.
Martins Pereira, S.L., Lobato, L.M., Ferreira, J.E., Jardim, E.C., 2007. Nature and origin of the BIF-hosted São Bento gold deposit, Quadrilátero Ferrífero, Brazil, with special emphasis on structural controls. Ore Geol. Rev. 32, 571–595.
Martins, B.S., Rosière, C.A., Lobato, L.M., Figueiredo e Silva, R.C., Baars, F.J., Tschiedel, M.W., et al., 2011. Mineralization control of the Lamego gold deposit, Sabará, Quadrilátero Ferrífero, Minas Gerais, Brazil. In: Applied, S.G. (Ed.), 11th SGA Biennial Meeting "Let's Talk Ore Deposits". Society Geology Applied, Antofagasta, Chile, pp. 583–585.
Noce, C.M., 1995. Geocronologia dos eventos magmáticos, sedimentares e metamórficos na região do Quadrilátero Ferrífero, Minas Gerais (PhD) Universidade de São Paulo, São Paulo.
Noce, C.M., Tassinari, C., Lobato, L.M., 2007. Geochronological framework of the Quadrilátero Ferrífero, with emphasis on the age of gold mineralization hosted in Archean greenstone belts. Ore Geol. Rev. 32, 500–510.
Noce, C.M., Zucchetti, M., Baltazar, O.F., Armstrong, R., Dantas, E., Renger, F., et al., 2005. Age of felsic volcanism and the role of ancient continental crust in the evolution of the Neoarchean Rio das Velhas Greenstone belt (Quadrilátero Ferrífero, Brazil): U–Pb zircon dating of volcaniclastic graywackes. Precambrian Res. 141, 67–82.
Oliveira, O.A.B., 1984. As falhas de empurrão e suas implicações na estratigrafia e metalogênese do Quadrilátero Ferrífero-MG. 34° Congresso Brasileiro de Geologia. Minas Gerais. pp. 1074–1187.
O'Rourke, J.E., 1957. The Stratigraphy of the Metamorphic Rocks of the Rio de Pedras and Gandarela Quadrangles, Minas Gerais, Brazil. University of Wisconsin, Wisconsin.
Paquette, J.-L., Nédélec, A., Moine, B., Rakotondrazafy, M., 1994. U–Pb, single zircon Pb-evaporation, and Sm–Nd isotopic study of a granulite domain in SE Madagascar. J. Geol. 523–538.
Pedreira, A.J., Silva, S.L., 1996. Sistemas deposicionais do greenstone belt Rio das Velhas, Quadrilátero Ferrífero, Minas Gerais. 39° Congresso Brasileiro de Geologia. Salvador, pp. 138–140.
Pedrosa-Soares, A., De Campos, C.P., Noce, C., Silva, L.C., Novo, T., Roncato, J., et al., 2011. Late Neoproterozoic-Cambrian granitic magmatism in the Araçuaí orogen (Brazil), the Eastern Brazilian Pegmatite Province and related mineral resources. Geol. Soc. Lond. Spec. Publ. 350, 25–51.
Percival, F., 1954. Sedimentary facies of iron formation. Econ. Geol. 49, 905.
Ramsay, J.Y.H., 1987. The Techniques of Modern Structural Geology, Volume 2: Folds and Fractures. Academic Press, London.
Ribeiro-Rodrigues, L.C., 1998. Gold in Archaen Banded Iron Formation of the Quadrilátero Ferrífero, Minas Gerais, Brazil — The Cuiabá Mine. Aachen University of Technology, Augustinus Verlag, Aachener Geowissenschaftliche Beiträge.
Ribeiro-Rodrigues, L.C., de Oliveira, C.G., Friedrich, G., 2007. The Archean BIF-hosted Cuiabá Gold deposit, Quadrilátero Ferrífero, Minas Gerais, Brazil. Ore Geol. Rev. 32, 543–570.
Robert, F., Poulsen, K.H., Cassidy, K.F., Hodgson, C.J., 2005. Gold metallogeny of the superior and Yilgarn Cratons. Econ. Geol. 100th Anniversary Volume, 1001–1034.
Salles, M., 1998. The Geological Setting of the Lamego Banded Iron-Formation-Hosted Gold Deposit. Ontario Queen's University, Quadrilátero Ferrífero District, Minas Gerais-Brazil.
Schorscher, H.D., 1988. NE Quadrilátero Ferrifero and adjacent areas. International Conference Geochemical Evolution of the Crust. Poços de Caldas, p. 1.
Seixas, L.A.R., David, J., Stevenson, R., 2012. Geochemistry, Nd isotopes and U–Pb geochronology of a 2350 Ma TTG suite, Minas Gerais, Brazil: implications for the crustal evolution of the southern São Francisco craton. Precambrian Res. 196, 61–80.
Stern, R.A., Rainbird, R.H., 2001. Advancements in xenotime U–Pb geochronology by ion microprobe. Eleventh Annual VM Goldschmidt Conference, p. 3872.
Stern, R., Sanborn, N., 1998. Monazite U–Pb and Th–Pb geochronology by high-resolution secondary ion mass spectrometry. Radiogenic age and isotopic studies: Report 11, pp. 1–18.
Teixeira, W., Ávila, C., Dussin, I., Neto, A.C., Bongiolo, E., Santos, J., et al., 2015. A juvenile accretion episode (2.35–2.32 Ga) in the Mineiro belt and its role to the Minas accretionary orogeny: zircon U–Pb–Hf and geochemical evidences. Precambrian Res. 256, 148–169.
Thorper, R.I., Cumming, G1., Kristic, D., 1984. Lead isotope evidence regarding age of gold deposits in the Nova Lima district, Minas Gerais, Brazil. Rev. Bras. Geosci. 14, 147–152.
Tomkins, A.G., Grundy, C., 2009. Upper temperature limits of orogenic gold deposit formation: constraints from the granulite-hosted Griffin's Find deposit, Yilgarn Craton. Econ. Geol. 104, 669–685.
Tomkins, A.G., Mavrogenes, J.A., 2002. Mobilization of gold as a polymetallic melt during pelite anatexis at the Challenger deposit, South Australia: a metamorphosed Archean gold deposit. Econ. Geol. 97, 1249–1271.
Tomkins, A.G., Pattison, D.R.M., Zaleski, E., 2004. The Hemlo Gold Deposit, Ontario: an example of melting and mobilization of a precious metal–sulfosalt assemblage during amphibolite facies metamorphism and deformation. Econ. Geol. 99, 1063–1084.
Vial, D., Abreu, G., Schubert, G., Ribeiro-Rodrigues, L., 2007a. Smaller gold deposits in the Archean Rio das Velhas greenstone belt, Quadrilátero Ferrífero, Brazil. Ore Geol. Rev. 32, 651–673.
Vial, D.S., DeWitt, E., Lobato, L.M., Thorman, C.H., 2007b. The geology of the Morro Velho gold deposit in the Archean Rio das Velhas greenstone belt, Quadrilátero Ferrífero, Brazil. Ore Geol. Rev. 32, 511–542.
Vial, D., Duarte, B., Fuzikawa, K., Vieira, M., 2007c. An epigenetic origin for the Passagem de Mariana gold deposit, Quadrilátero Ferrífero, Minas Gerais, Brazil. Ore Geol. Rev. 32, 596–613.
Vieira, F.W.R., 1991. Textures and processes of hydrothermal alteration and mineralization in the Nova Lima Group, Minas Gerais, Brazil. In: Ladeira, E.A. (Ed.), Brazil Gold'91. Gold, Belo Horizonte, pp. 319–327.
Villanova, F.L.S.P., 2011. Mapeamento Geológico em escala 1:5.000 da superfície e região circunvizinha da Mina Lamego, Sabará, Minas Gerais. Trabalho Geológico de Graduação, p. 80.
Vollgger, S.A., Cruden, A.R., Cowan, J.E., 2013. 3D implicit geological modeling of a gold deposit from a structural geologist's point of view. In: Applied, S.G. (Ed.), 12th SGA Biennial Meeting — Mineral Deposit Research for a High-Tech World. SGA, Uppsala, Sweden.
Wilkinson, J.J., Boyce, A.J., Earls, G., Fallick, A.E., 1999. Gold remobilization by low-temperature brines: evidence from the Curraghinalt gold deposit, Northern Ireland. Econ. Geol. 94, 289–296.